Meeting Report on the 13th International Conference on Human Retrovirology: Human T-Cell Leukemia Virus Research 30 Years after Adult T-Cell Leukemia

Masao Matsuoka,[1] Toshiki Watanabe,[2] Mari Kannagi,[3] Charles Bangham,[4] Ralph Grassmann,[5] Susan J. Marriott,[6] Patrick Green,[7] and Kuan-Teh Jeang[8]

[1]Institute for Virus Research, Kyoto University, Kyoto, Japan; [2]Laboratory of Tumor Cell Biology, University of Tokyo and [3]Department of Immunotherapeutics, Tokyo Medical and Dental University, Tokyo, Japan; [4]Department of Immunology, Imperial College Faculty of Medicine, London, United Kingdom; [5]Institute of Clinical and Molecular Virology, University Erlangen-Nuremberg, Erlangen, Germany; [6]Department of Molecular Virology and Microbiology, Baylor College of Medicine, Houston, Texas; [7]Department of Veterinary Biosciences, Ohio State University, Columbus, Ohio; and [8]Laboratory of Molecular Microbiology, National Institute of Allergy and Infectious Diseases, Bethesda, Maryland

Introduction

Thirty years ago, in 1977, a new clinical entity called adult T-cell leukemia (ATL) was described in Japan by Takatsuki and colleagues. Subsequently, Poiesz, Ruscetti, Gallo, and coworkers; and Yoshida, Miyoshi, Hinuma, and colleagues isolated a human retrovirus named human T-cell leukemia virus type-1 (HTLV-1). The history of the discovery of ATL and the isolation of HTLV-1 has been recently reviewed elsewhere (1–3).

From May 22 to 25, 2007, 350 researchers gathered in Hakone, Japan, at the 13th International Conference on Human Retrovirology organized by Toshiki Watanabe (University of Tokyo, Tokyo, Japan) to discuss the latest finding on HTLV-1 pathogenesis. The meeting opened with a keynote presentation by Kuan-Teh Jeang [National Institute of Allergy and Infectious Diseases (NIAID), Bethesda, MD] reviewing cell proliferative changes, genetic damaging events, and check point inactivation in the development of ATL (4). Over the next 4 days, >320 papers were presented. Conference highlights are summarized below.

Epidemiology of HTLV

HTLV infects 10 to 20 million individuals worldwide. Masahiro Satake (Tokyo Red Cross Blood Center, Tokyo, Japan) reported on HTLV-1 positivity rate (0.37%) in Japanese first-time blood donors. HTLV-1 seropositivity in donors was 1.18% in their 30s in 1995 and 1.28% in their 40s in 2005, showing an 8% increase in 10 years. The same trend was found in the donors who were an additional 10 years older. Satake interpreted these figures to reveal the rate of horizontal infection in Japan. How individuals become susceptible to HTLV infection was commented upon by Sabine Plancoulaine [Institut National de la Sante et de la Recherche Medicale (INSERM), Paris, France] using a genome-wide linkage analysis mapping the susceptibility locus in children of African origin for HTLV-1 infection through breast feeding. She found significant linkage between HTLV-1 susceptibility and two chromosomal loci at 2p25 and 6q27.

HTLV-1 infection is also associated with an inflammatory pathology termed HTLV-associated myelopathy (HAM) or tropical spastic paraparesis (TSP). The association of neurologic abnormalities and HTLV-1 infection was discussed by Edward Murphy (University of California San Francisco, San Francisco, CA). In his study (HTLV Outcome Study), Murphy followed 151 HTLV-1–positive and 387 HTLV-2–positive former blood donors for 10 years (5). Compared with uninfected controls, HTLV-positive subjects had significantly more motor and coordination abnormalities. Murphy concluded that HTLV-1 and HTLV-2 infections are associated with a spectrum of neurologic defects beyond those described previously for classic HAM.

Tax, Transcription, Cellular Proliferation, and Transformation

The HTLV-1 Tax oncoprotein induces cellular proliferation, survival, and genetic damage. Nuclear factor-κB (NF-κB) has been described as an important cellular target activated by Tax through both the canonical and noncanonical pathways. Masahiro Fujii (Niigata University, Niigata, Japan) suggested in new findings a specificity of noncanonical NF-κB activation in HTLV-1 pathogenesis. He found that noncanonical activation of NF-κB, as measured by p52 processing from its p100 precursor, is restricted to HTLV-1, but not HTLV-2, Tax. Interestingly, HTLV-1, but not HTLV-2, is oncogenic. Fujii further reported that noncanonical NF-κB activation depends on the PDZ binding motif (PBM) of Tax1 (located in carboxyl-terminal amino acids 350–353).

Following-up on the role of Tax PBM, complete genome sequences from two recently isolated African HTLVs, HTLV-3 (Sara Calattini and Renaud Mahieux, Pasteur, Paris, France) and HTLV-4 (William Switzer, Centers for Disease Control and Prevention, Atlanta, GA), were presented. The data revealed that HTLV-3 Tax retains a PBM that is absent from HTLV-4 Tax. This observation predicts different pathogenic outcomes from HTLV-3 and HTLV-4 infections.

Two presentations addressed Tax and genetic instability. Susan Marriott (Baylor College of Medicine, Houston, TX) reported that Tax represses double-strand DNA repair, which is partly governed by a protein complex containing DNA-protein kinase (DNA-PK). John Semmes (Eastern Virginia University, Norfolk, VA) showed that Tax binds DNA-PK directly and sequesters this factor into nuclear speckles, thus repressing double-strand DNA repair.

Note: The 13th International Conference on Human Retrovirology was held from May 22–25, 2007 in Hakone, Japan.

Requests for reprints: Kuan-Teh Jeang, Laboratory of Molecular Microbiology, National Institute of Allergy and Infectious Diseases, Building 4, Room 306, 9000 Rockville Pike, NIH, Bethesda, MD 20892-0460. Phone: 301-496-6680; Fax: 301-480-3686; E-mail: kj7e@nih.gov.

doi:10.1158/0008-5472.CAN-07-2587

Tax can affect host cell metabolism through transcriptional activation of cellular genes. Jennifer Nyborg (Colorado State University, Fort Collins, CO) found that Tax promotes cyclic AMP–responsive element binding protein (CREB) phosphorylation, increasing the availability of modified CREB for promoter transactivation. Paul Laybourn (Colorado State University) identified a new function of Tax abrogation of H1-mediated repression of p300 coactivator activity. Laybourn also found that Tax decreased histone mRNA levels, arguing that such reduction may contribute to dysregulated expression of many cellular genes. Additional insight into Tax activation of promoters was provided by Nicholas Polakowski and Isabelle Lemasson (East Carolina University, Greenville, NC) who used a chromatin immunoprecipitation assay/microarray (ChIP-on-CHIP) approach to describe direct recruitment of Tax to many cellular promoters.

What are some of these promoters? Cynthia Pise-Masison's [National Cancer Institute (NCI), Bethesda, MD] microarray analyses revealed increased expression in ATL leukemic cells of genes linked to cell cycle progression (e.g., *CDC2, CCN1*), apoptosis repression (e.g., survivin), and tyrosine kinases (e.g., Lyn). Separately, Ralph Grassmann (University of Erlangen-Nuremberg, Erlangen, Germany) and Kuan-Teh Jeang (NIAID) showed altered microRNA (miRNA) expression in HTLV-1–transformed cells, suggesting that Tax also affects/occupies promoters that transcribe oncogenic miRNAs.

Many questions pertaining to *in vivo tax* and virus expression are currently unanswered. Charles Bangham (Imperial College, London, United Kingdom) used deuterated glucose for labeling patients' lymphocytes to check the *in vivo* effect of *tax*/HTLV expression on lymphocyte population dynamics. He saw increased proliferation of $CD4^+CD45RO^+$ and $CD8^+CD45RO^+$ T-lymphocytes in HTLV-1–infected persons compared with controls, with the additional production of 10^{12} lymphocytes per year in the former. The *in vivo* proliferation rate of $CD4^+CD45RO^+$ cells correlated with *tax* expression (measured *ex vivo*), supporting a physiologic role (directly or indirectly) for this viral oncoprotein in the proliferation of infected cells (6).

Functional Contributions from HTLV Accessory Genes

Besides *gag, pol, env*, and *tax*, HTLV encodes *rex* and accessory genes *hbz, p12, p13, p27*, and *p30*. Agnes Lezin (Fort-De-France, Martinique) quantified the expression levels of the HTLV-1 accessory genes in primary cells from HAM/TSP, ATL, and asymptomatic patients. She reported that that *p12, p27*, and *p30* expression was undetectable whereas levels of *tax, hbz*, and *p13* transcripts quantitatively correlated with clinical progression.

HTLV-1 HBZ is unique among viral proteins in being encoded by the minus strand of the provirus. Published studies suggested that *hbz* can function as an RNA and as a protein. At this meeting, Masao Matsouka (Kyoto University, Kyoto, Japan) mapped HBZ proliferative activity to the 5′ end of its RNA. His transgenic mice constructed to express *HBZ* gene driven by the mouse CD4 promoter/enhancer showed increased $CD4^+$ T cells in the spleen with infiltration into the skin and lung. Osamu Isono (Kyoto University) presented evidence that HBZ protein represses c-Jun activity by destabilizing c-Jun and promoting its proteosomal degradation. Jean-Michel Mesnard (Centre National de la Recherche Scientifique, Montpellier, France) had previously published that HBZ protein stimulates JunD activity. Following up on that finding, Sophie Kuhlmann (INSERM, Lyon, France) reported that HBZ/JunD interaction upregulates expression of the *human telomerase reverse transcriptase* gene, potentially explaining elevated telomerase activity in ATL cells.

The p30 protein promotes replication and persistence of HTLV-1 by acting at transcriptional and posttranscriptional levels. Veffa Franchini (NCI) used an infectious proviral clone to show the action of p30 in posttranscriptional gene repression. She showed that deletion of p30 from the provirus increased Tax expression and HTLV-1 replication. Michael Lairmore (Ohio State University, Columbus, OH) followed with data that added complexity to p30 function. He found increased phosphorylation of cell cycle regulators Cdc25C and Chk1 in Jurkat T-cells expressing p30, and p30 association with nuclear γ-H2AX DNA-repair foci. Lairmore proposed a role for p30 in signaling DNA damage (perhaps triggered by retroviral integration).

HTLV-1 p13 and Rex were also discussed at this meeting. Vincenzo Ciminale showed that p13 expression increased mitochondrial reactive oxygen species, influencing the metabolism of the cell by favoring aerobic metabolism, and moderating apoptosis. Patrick Green (Ohio State University) discussed that the phosphorylation status of HTLV-2 Rex at its COOH terminus is important for protein stability and function. Phosphomimetic Rex mutants were shown to be constitutively active, and these Rex mutant viruses displayed increased viral replication both *in vitro* and in inoculated rabbits. However, Rex mutant viruses were similar to wild-type virus in the capacity to immortalize T lymphocytes in culture and persist in infected rabbits.

Immunologic Implications of Viral Infection

Inflammatory lesions in HAM/TSP are associated with the breakdown of the blood-brain barrier. The factors that cause the breakdown of the blood-brain barrier are not known. Philippe Afonso (Pasteur Institute, Paris, France) showed that HTLV-1–infected lymphocytes could induce an increase in both paracellular endothelial permeability and transcellular migration in an *in vitro* model of the blood-brain barrier. The observed changes were accompanied by disruption of intercellular tight junctions and seemed to be mediated by interleukin (IL)–1 and tumor necrosis factor-α.

HTLV-1 Tax induces strong expression of the high-affinity IL-2Rα chain (CD25) on the infected $CD4^+$ T cell. CD25 is also characteristically expressed at a high level on the malignantly transformed $CD4^+$ T cells in ATL. These observations have stimulated considerable interest because certain $CD4^+$ $CD25^+$ T cells, known as regulatory T cells (T_{regs}), can suppress the proliferation and function of other T cells. It is now becoming clear that the intracellular expression of the transcriptional factor FoxP3 in $CD4^+$ T cells is more strongly associated with a T_{reg} phenotype than is CD25 expression, because CD25 is also characteristically expressed on activated T cells. Because of the expression of both CD25 and, in a proportion of cases, FoxP3 in ATL cells, questions have recently been raised whether HTLV-1 preferentially infects or transforms $CD4^+$ $CD25^+$ $FoxP3^+$ T cells (Shimeru Kamihira, Nagasaki University, Nagasaki, Japan) and whether the ATL cells themselves act as T_{regs}. The latter

is an important possibility because ATL is characterized by even more profound immunosuppression than is seen in other leukemias.

Hiroki Yano (Nagoya City University, Nagoya, Japan) tested the ability of ATL cells (identified by a receptor frequently coexpressed on ATL cells, CCR4) to inhibit the proliferation of autologous $CD4^+$ non-ATL cells. In five ATL cases studied, evidence was obtained of a degree of suppression in one case, and suggestive evidence was obtained in one further case. Frederic Toulza (Imperial College, London, United Kingdom) used a simple phenotypic definition of T_{reg} cells, $CD4^+$ $FoxP3^+$, and reported that the percentage of $CD4^+$ $FoxP3^+$ cells in the circulation was negatively correlated with the rate of lysis of autologous naturally infected $CD4^+$ T cells by the patient's $CD8^+$ CTLs. The results suggest that $CD4^+$ $FoxP3^+$ cells play a major role in determining the efficiency of CTL surveillance of HTLV-1. Because there is increasing evidence that the CTL response to this virus determines the proviral load and the risk of inflammatory disease, it is possible that T_{regs} are an important determinant of the outcome of HTLV-1 infection.

Mari Kannagi (Tokyo Medical and Dental University, Tokyo, Japan) reported that immunization of orally infected rats with syngeneic, mitomycin C–treated HTLV-1–transformed cells boosted the cellular immune response to HTLV-1, and that this strengthened immune response was accompanied by a reduction in the proviral load (7). Charles Bangham has evidence for abnormally rapid turnover *in vivo* of both HTLV-1–infected $CD4^+$ T cells and $CD8^+$ T cells (which include the HTLV-1–specific CTLs; ref. 6) with a typical HTLV-1–infected individual turning over an extra 10^{12} lymphocytes per year. Thus, the findings from rats (7) and humans (6) lend weight to the growing evidence that HTLV-1 does not rely solely on latency to persist. Rather, HTLV-1 infection seems to be a highly dynamic equilibrium between persistent viral expression and the immune response.

Therapeutic Approaches to HTLV-1 Infection

Several speakers reviewed various ATL treatment options. Deidre O'Mahony (NCI) presented a phase 1 trial of Splizumab, a monoclonal antibody that binds to CD2 on human T-cells and natural killer cells, in CD2-positive lymphoid malignancies, including aggressive ATL with early encouraging response rates and relatively low toxicities. Lee Ratner (Washington University, St. Louis, MO) reported mixed clinical and virological findings from etoposide, prednisone, vincristine, cyclophosphamide, and doxorubicin (EPOCH) infusional chemotherapy followed by zidovudine and interferon-α. Low levels of viral RNA were seen at the initiation of therapy, but viral RNA levels increased >10-fold in most relapsed cases during therapy. Juan Carlos Ramos (University of Miami, Miami, FL) found that the expression of IRF-4/MUM-1 and c-Rel in the absence of Tax in primary ATL cells was associated with resistance to zidovudine and interferon-α treatment.

Impressive treatment efficacy was seen from reduced-intensity stem cell transplantation (RIST) as reported by Ryuji Tanosaki (National Cancer Center Hospital, Tokyo, Japan). Among 18 patients who received RIST, 14 patients achieved complete remission. Three-year overall survival and event-free survival were 67 ± 12% and 55 ± 12%, respectively. Further explaining why stem cell transplantation is effective for ATL, Nanae Harashima (Tokyo Medical and Dental University) reported that Tax-specific CTL response was recovered [by stimulating peripheral blood mononuclear cells (PBMC) *in vitro* with HTLV-1–infected cells] after stem cell transplantation, suggesting a role for CTL in eliminating Tax-expressing cells and preventing relapse of ATL.

Seishi Ogawa and Toshiki Watanabe (University of Tokyo) described molecular allelo-karyotyping of primary ATL cells using high single-nucleotide polymorphism genotyping microarrays. ATL lymphoma-type genomes from 108 patients showed characteristic copy number profiles and unique patterns of allelic imbalances. Future detailed molecular investigation of these results could reveal novel drug targets for ATL treatment.

For TSP/HAM treatment, Agnes Lézin (Fort-De-France, Martinique) is investigating the use of histone deacetylase inhibitors, valproate, to activate the expression of latent HTLV-1 proviruses *in vivo* and expose the activated infected cells to CTL immune surveillance. Lézin reported that valproate induced a significant reduction of provirus loads (mean 24-fold) in HAM/TSP patients.

Development of Mouse Models for HTLV-1 and ATL

To date, oncogenic potential of Tax in transgenic mice has been intensively studied. However, all extant lymphoid and nonlymphoid tumors in mice have lacked the CD4 surface marker. By contrast, CD4 is present on almost all patient ATL cells. Hideki Hasegawa (National Institute of Infectious Diseases, Tokyo, Japan) had published recently that transgenic mice expressing Tax driven by a lymphocyte-specific protein tyrosine kinase Lck-proximal promoter, targeting immature thymocytes, developed $CD4^-$ $CD8^-$ double-negative pre–T-cell leukemia/lymphoma (8). In new findings using the distal *lck* promoter, Takeo Ohsugi and Toru Urano (Kumamoto University, Kumamoto, Japan) now reported a *tax* transgenic mouse, which developed $CD4^+$ T-cell leukemia (9).

It is popular to use nonobese diabetic severe combined immunodeficient (NOD-SCID) common γ-chain null (NOG) mice for transplantation with human cells. Paola Miyazato (Kyoto University) showed that spread of HTLV-1 infection in human PBMCs transplanted into NOG mice could be blocked by azidothymidine and tenofovir but only in early stages of infection. She discussed that Tax mRNA expression in the infected human cells in NOG mice increased after *in vitro* culture, similar to that seen in human cases. In a related approach, Prabal Banerjee (State University of New York, Syracuse, NY) explanted HTLV-1–infected human $CD34^+$ hematopoietic progenitor cells into NOD-SCID mice. He observed HTLV-1–infected human T cells, B cells, and monocytes/macrophages in transplanted mice. Some of the mice showed proliferation of HTLV-1–infected $CD4^+$ T cell in lymphoid tissues as well as HTLV-1–infected $CD34^+$ cells persisting in the bone marrow and thymus. Banerjee also reported that reconstitution of NOD-SCID mice with HTLV-1 Tax-transduced human $CD34^+$ cells produced proliferating $CD4^+$ T cells.

Future Perspectives

In the 30 years since the description of ATL, much has been learnt about HTLV-1 pathogenesis. Going forward, several important questions remain to be addressed for oncological research on ATL. Will the next years bring clarifying insights into roles contributed by human miRNAs to ATL initiation and progression? Will we learn

why Tax is dispensable for ATL maintenance and why ATL does not use the "oncogene addiction" model of transformation? Will findings of virus-induced senescence, checkpoint inactivation, and cellular genetic damage meld into a coherent chronology of transformation events? In addition to these questions, equally important topics challenge immunologic and clinical HTLV-1 research. Indeed, one can look with anticipation to many intriguing answers that await revelation over the next 30 years.

Acknowledgments

Received 7/10/2007; revised 7/30/2007; accepted 9/10/2007.

References

1. Takatsuki K. Discovery of adult T-cell leukemia. Retrovirology 2005;2:16.
2. Gallo RC. The discovery of the first human retrovirus: HTLV-1 and HTLV-2. Retrovirology 2005;2:17.
3. Yoshida M. Discovery of HTLV-1, the first human retrovirus, its unique regulatory mechanisms, and insights into pathogenesis. Oncogene 2005;24:5931–7.
4. Matsuoka M, Jeang KT. Human T-cell leukaemia virus type 1 (HTLV-1) infectivity and cellular transformation. Nat Rev Cancer 2007;7:270–80.
5. Kwaan N, Lee TH, Chafets DM, et al. Long-term variations in human T lymphotropic virus (HTLV)-I and HTLV-II proviral loads and association with clinical data. J Infect Dis 2006;194:1557–64.
6. Asquith B, Zhang Y, Mosley AJ, et al. *In vivo* T lymphocyte dynamics in humans and the impact of human T-lymphotropic virus 1 infection. Proc Natl Acad Sci U S A 2007;1048035–40.
7. Komori K, Hasegawa A, Kurihara K, et al. Reduction of human T-cell leukemia virus type 1 (HTLV-1) proviral loads in rats orally infected with HTLV-1 by reimmunization with HTLV-1-infected cells. J Virol 2006;80:7375–81.
8. Hasegawa H, Sawa H, Lewis MJ, et al. Thymus-derived leukemia-lymphoma in mice transgenic for the Tax gene of human T-lymphotropic virus type I. Nat Med 2006;12:466–72.
9. Ohsugi T, Kumasaka T, Okada S, Urano T. The Tax protein of HTLV-1 promotes oncogenesis in not only immature T cells but also mature T cells. Nat Med 2007;13:527–8.

Laboratory Investigation (2007) 87, 372–382

IκBα independent induction of NF-κB and its inhibition by DHMEQ in Hodgkin/Reed-Sternberg cells

Mariko Watanabe[1,*], Md Zahidunnabi Dewan[2,3,*], Miyako Taira[1], Momoko Shoda[4], Mitsuo Honda[3], Testutaro Sata[5], Masaaki Higashihara[1], Marshall E Kadin[6], Toshiki Watanabe[4], Naoki Yamamoto[2,3], Kazuo Umezawa[7] and Ryouichi Horie[1]

Constitutive nuclear factor κB (NF-κB) activation characterizes Hodgkin/Reed-Sternberg (H-RS) cells. Blocking constitutive NF-κB has been shown to be a potential strategy to treat Hodgkin lymphoma (HL). Here, for the first time we show that although constitutive NF-κB level of H-RS cell lines is very high, topoisomerase inhibitors further enhance NF-κB activation through IκB kinase activation in not only H-RS cell lines with wild-type IκBα, but also in those with IκBα mutations and lacking wild-type IκBα. Thus, both constitutive and inducible NF-κB are potential targets to treat HL. We also present the data that indicate the involvement of IκBβ in NF-κB induction by topoisomerase inhibitors. A new NF-κB inhibitor, dehydroxymethylepoxyquinomicin (DHMEQ) inhibited constitutive NF-κB activity and induced apoptosis of H-RS cell lines. DHMEQ also inhibited the growth of H-RS cells without significant systemic toxicity in a NOD/SCID/γc^{null} (NOG) mice model. DHMEQ and topoisomerase inhibitors revealed enhancement of apoptosis of H-RS cells by blocking inducible NF-κB. Results of this study suggest that both constitutive and inducible NF-κB are molecular targets of DHMEQ in the treatment of HL. The results also indicate that IκBβ is involved in NF-κB activation in H-RS cells and IκBβ substitutes for IκBα in H-RS cells lacking wild-type IκBα.
Laboratory Investigation (2007) **87**, 372–382. doi:10.1038/labinvest.3700528; published online 19 February 2007

KEYWORDS: DHMEQ; Hodgkin lymphoma; IκBα mutation; NF-κB; topoisomerase inhibitors

Advances in chemotherapy and radiotherapy regimens for treating Hodgkin lymphoma (HL) represent a significant breakthrough in clinical oncology and have increased the long-term survival rate from 5% in the 1960s to greater than 80%. Today, problems of late side effects by chemotherapy such as secondary malignancies, myelodysplasia and cardiotoxicities and chemotherapy-resistant cases with poor prognosis have become important issues to still be resolved.[1] Recently, a strategy that targets the molecules critical for maintenance and growth of the tumor cells has been thought to be a key to develop more effective treatment with less undesirable effects.[2] This strategy intensifies the specificity of treatments to tumor cells and minimizes undesirable effects to normal cells. To establish a molecular target strategy for HL, it appears critical to identify the biological basis involved in anti-apoptosis of HL and develop specific agents that target this pathway.

It was found that constitutively activated nuclear factor-κB (NF-κB) is a molecular hallmark and survival mechanism for Hodgkin/Reed–Sternberg (H-RS) cells. Defective IκBα has been reported to be a cause of constitutive NF-κB activation in H-RS cells bearing IκBα gene mutations.[3–7] We also reported that ligand-independent signals from overexpressed CD30 is responsible for constitutive NF-κB activation.[8]

[1]Department of Hematology, School of Medicine, Kitasato University, Kitasato, Sagamihara, Kanagawa, Japan; [2]Department of Molecular Virology, Graduate School, Tokyo Medical and Dental University, Yushima, Bunkyo-ku, Tokyo, Japan; [3]AIDS Research Center, National Institute of Infectious Diseases, Toyama, Shinjuku-ku, Tokyo, Japan; [4]Laboratory of Tumor Cell Biology, Department of Medical Genome Sciences, Graduate School of Frontier Sciences, The University of Tokyo, Shirokanedai, Minato-ku, Tokyo, Japan; [5]Department of Pathology, National Institute of Infectious Diseases, Toyama, Shinjuku-ku, Tokyo, Japan; [6]Department of Pathology, Harvard Medical School and Beth Israel Deaconess Medical Center, Boston, MA, USA and [7]Department of Applied Chemistry, Faculty of Science and Technology, Keio University, Hiyoshi, Kohoku-ku, Yokohama, Kanagawa, Japan

Correspondence: Dr R Horie, MD, PhD, Department of Hematology, School of Medicine, Kitasato University, 1-15-1 Kitasato, Sagamihara, Kanagawa 228-8555, Japan. E-mail: rhorie@med.kitasato-u.ac.jp or

Dr N Yamamoto, MD, PhD, Department of Molecular Virology, Graduate School, Tokyo Medical and Dental University, 1-5-45 Yushima, Bunkyo-ku, Tokyo 113-8519, Japan.

E-mail: yamamoto.mmb@tmd.ac.jp

*These authors contributed equally to this work.

Received 20 May 2006; revised 25 November 2006; accepted 16 December 2006

Constitutively activated NF-κB is considered to be responsible for aberrant growth and cytokine gene expression of H-RS cells.[9,10] We reported that adenovirus-mediated gene transfer of a dominant IκBα resistant to phosphorylation-mediated degradation or a decoy CD30 lacking a tumor necrosis factor receptor associated factor (TRAF) binding domain can block the constitutive NF-κB activity and induce apoptosis in H-RS cell lines.[8] These observations suggest that NF-κB, which is strongly and constitutively activated in H-RS cells, provides a molecular target for the treatment of HL.

Recently, NF-κB activation has also been connected with chemo-resistance of tumor cells.[11] Topoisomerases are essential for cell survival and crucial for multiple aspects of DNA metabolism. Topoisomerases control the degree of supercoiled DNA, and whereas type I is crucial for transcription, type II is necessary for DNA replication. In both situations, the enzyme creates transient single-strand breaks in DNA, and the inhibitors prevent the replication of the strand breaks. SN-38, a powerful active metabolite of CPT-11, targets topoisomerase I activity, whereas daunorubicin and etoposide are topoisomerase II inhibitors. Treatments with topoisomerase inhibitors induce transient NF-κB activation via IκB kinase (IKK), which makes tumor cells resistant to induction of apoptosis.[12]

Previous reports suggested that blockade of the SN-38-induced activation of NF-κB by adenovirus-mediated gene transfer of IκBα super-repressor enhanced anti-tumor activity.[13] Therefore, if topoisomerase inhibitors induce NF-κB activation in H-RS cells, inducible NF-κB also becomes a potential molecular target to treat HL. As tumor cells used in previous experiments did not show constitutive NF-κB activity, it remains to be examined whether the same strategy can be applied to tumor cells of HL with constitutive activation of NF-κB, especially for those with IκBα mutations.

IκBα mutations result in production of truncated, non-functional IκBα protein. Existence of IκBα mutations and lack of wild-type IκBα has been thought to make NF-κB activity uncontrolled by upstream IKK signals, leading to constitutive activation of NF-κB.[3–5,7] NF-κB induction by topoisomerase inhibitors has been reported to be mediated by IKK.[12,14] Therefore, it can be hypothesized that treatment with topoisomerase inhibitors will fail to induce NF-κB activity in H-RS cell lines with IκBα mutations.

Dehydroxymethylepoxyquinomicin (DHMEQ) is a new NF-κB inhibitor that is 5-dehydroxymethyl derivative of a novel compound epoxyquinomicin C having a 4-hydroxy-5,6-epoxycyclohexenone structure like panepoxydone.[15] Panepoxydone had been found to inhibit TNF-α-induced activation of NF-κB. We have shown that DHMEQ inhibits NF-κB at the level of nuclear translocation.[15]

In the present study, we demonstrate that topoisomerase inhibitors induce NF-κB in not only H-RS cell lines with wild-type IκBα but also in H-RS cell lines lacking wild-type IκBα by activating IKK and constitutive as well as inducible NF-κB are the molecular target of HL treatment by DHMEQ. The results also indicate that NF-κB activity in H-RS cells with IκBα mutations is regulated by IκBβ, which is a substitute for IκBα.

MATERIALS AND METHODS

Cell Cultures

H-RS cell lines (KMH2, L428, HDLM2 and L540) were purchased from the German Collection of Microorganisms and Cell Cultures (Braunschweig, Germany). Cell lines were cultured in RPMI 1640 with supplementation of recommended concentrations of fetal bovine serum (FBS) and antibiotics. Peripheral blood mononuclear cells (PBMC) obtained from healthy volunteers were cultured in RPMI 1640 supplemented with 20% FBS and antibiotics.

Chemicals

DHMEQ is a NF-κB inhibitor that acts at the level of nuclear translocation of NF-κB.[15,16] Daunorubicin and etoposide were purchased from SIGMA (Toyko, Japan). SN-38, an active metabolite of camptothecin-11, was provided by Yakult (Tokyo, Japan). Compounds were dissolved with DMSO and used for experiments at the indicated concentrations. Bisbenzimide H 33342 fluorochrome (Hoechst 33342) was purchased from CALBIOCHEM (Bad Soden, Germany).

Electrophoretic Mobility Shift Analysis

Electrophoretic mobility shift analysis (EMSA) was carried out according to the methods described previously.[17] Double-stranded oligonucleotide probes containing the mouse immunoglobulin kappa (Igκ) light-chain NF-κB consensus site and Oct-1 were purchased from Promega (Madison, WI, USA). Antibodies used for super-shift assays were as follows: NF-κB p50 (C-19) goat polyclonal antibody, RelB (C-19) rabbit polyclonal antibody and mouse antibodies for NF-κB p65 (C-20), NF-κB p52 (C-5) and c-Rel (B-6) (all from Santa Cruz Biotechnology, Inc., Santa Cruz, CA, USA).

In Vitro Kinase Assay

Cell extracts prepared from equivalent numbers of cells were subjected to immunoprecipitation with anti-IKKα monoclonal antibody in TNT buffer (20 mM TrisHCl (pH 7.5), 200 mM NaCl, 1% Triton X100, 0.5 mM PMSF, 1 mg/ml leupeptin, 1 mg/ml aprotinin, 100 μM Na_3VO_4 and 20 mM β-glycerophosphate). Immunoprecipitates were collected on Protein G-Sepharose beads (Amersham Biosciences Corp., Piscataway, NJ, USA), which were then washed three times with TNT buffer and three times with kinase reaction buffer (20 mM HEPES (pH 7.5), 10 mM $MgCl_2$, 50 mM NaCl, 100 μM Na_3VO_4, 20 mM β-glycerophosphate, 2 mM DTT, and 20 mM ATP). Kinase reactions were performed for 30 min at 30°C using 5 μCi of [γ-^{32}P]ATP and glutathione S-transferase (GST)-IκBα protein (amino acids 1317) (Santa Cruz Biotechnology, Inc.) as substrates. The reaction products were separated on 12% sodium dodecyl sulfate (SDS)–polyacrylamide gels and revealed by autoradiography.

Antibodies for IKKα (B78-1) (BD Biosciences Pharmingen, San Diego, CA, USA) and IKKα/β (H-470) (Santa Cruz Biotechnology, Inc.) were used for immunoprecipitation and immunoblot of IKKα respectively.

Coimmunoprecipitation Analysis

Cell extracts were subjected to immunoprecipitation with anti-IκB-β (S-20) rabbit polyclonal antibody (Santa Cruz Biotechnology, Inc.) in TNE buffer (10 mM Tris–HCl, pH 7.8, 1% Nonidet P-40, 150 mM NaCl, 1 mM EDTA). Immunoprecipitates were collected on Protein G-Sepharose beads (Amersham Biosciences Corp.), which were then washed three times with TNE buffer.

Immunoblot Analysis

Immunoblot analysis was performed as described.[17] Antibodies used were as follows: NF-κB p65 (F-6) mouse monoclonal antibody, NF-κB p50 (C-19) gout polyclonal antibody, IκB-β(S-20) rabbit polyclonal antibody, α tubulin (TU-02) mouse monoclonal IgM antibody (all from Santa Cruz Biotechnology, Inc.) and phosphoserine mouse monoclonal IgM antibody (Biomol, Meeting, PA, USA). Alkaline phosphatase-conjugated secondary antibodies are as follows: donkey anti-goat IgG antibody, donkey anti-mouse IgG antibody, donkey anti-rabbit IgG antibody (all from Chemicon International, Temecula, CA, USA) and goat anti-mouse IgM antibody (Santa Cruz Biotechnology, Inc.).

Cell Viability Assay

Effects of DHMEQ on cell viability were assayed by the MTT method as described previously.[8] After incubation with DHMEQ or DMSO alone at the indicated concentrations and time points, 5×10^4 cells treated with MTT solution were measured by a microplate reader (Bio-Rad, Richmond, CA, USA) at a reference wavelength of 570 nm and test wavelength of 450 nm. The cell viability was expressed as a percentage of the DMSO-treated control samples.

Immunohistochemistry

Immunohistochemical analyses were carried out as described.[17] Primary antibodies used were as follows: mouse monoclonal antibody for activated NF-κB p65 (Chemicon International), rabbit polyclonal antibodies for cleaved caspase-3 (Asp-175) (Cell signalling, Beverly, MA, USA), NF-κB p65 (C-20), Bcl-xL (H-62), FLIPs/l (H-202), GAPDH (FL-335) and mouse monoclonal antibody for α tubulin (TU-02) (all from Santa Cruz Biotechnology, Inc.). Fluorochrome-labeled secondary antibodies used in these studies are as follows: FITC-labeled anti-goat immunoglobulin donkey antibody, FITC-labeled anti-rabbit immunoglobulin goat antibody and FITC-labeled anti-mouse immunoglobulin goat antibody (all from Santa Cruz Biotechnology, Inc.).

Northern Blotting

Northern blot analysis was carried out essentially as described.[17] Briefly, 2 μg of poly(A)-selected RNA was size-fractionated on 1% formalin agarose gel electrophoresis and subsequently blotted onto Hybond-C extra-nitrocellulose membranes (Amersham Bioscience Corp.). Filters were hybridized in 4 × SSC, 1 × Denhardts, 0.5% SDS, 0.1 M $NaPO_4$ (pH 7.0), 10% Dextran-Na at 65°C with 1.0×10^6 cpm/ml of random prime-labeled probes. After washings to a final stringency of 0.2 × SSC and 0.1% SDS at 65°C, filters were exposed to XAR-5 films (Eastman Kodak, Rochester, NY, USA) at −80°C. RT-PCR amplified cDNA fragments of human Bcl-xL, human FLIPs/l and human GAPDH were used as probes.

Apoptosis and Analysis of Caspase Activity

Cells were labeled with FITC-conjugated Annexin V (BD Biosciences, Pharmingen) and followed by flow cytometric analysis. For analysis of morphological changes of nuclei, cells were stained by 10 μM Hoechst 33342, and photographed through a UV filter. Activation of caspases was examined by detecting decrease of uncleaved fragments or appearance of cleaved fragments with immunoblot analysis. Antibodies used in these experiments were as follows: mouse monoclonal antibodies for caspase-3/CPP32 (BD Biosciences Pharmingen), cleaved caspase-8 (Asp384) 11G10 and rabbit polyclonal antibodies for caspase-9 (both from Cell Signaling). Alkaline phosphatase-conjugated secondary antibodies are as follows: anti-mouse IgG (H&L) antibody and anti-rabbit IgG (Fc) antibody (both from Promega). caspase activity was blocked using cell-permeable irreversible caspase-3 inhibitor II (z-DEVD-FMK), caspase 8 inhibitor II (z-IETD-FMK) or caspase-9 inhibitor I (z-LEHD-FMK) (all from CALBIOCHEM).

In Vivo Therapeutic Effect of DHMEQ

NOG mice were purchased from the Central Institute for Experimental Animals (Kawasaki, Japan). The Ethical Review Committee of the National Institute of Infectious Diseases approved the experimental protocol. H-RS cells were inoculated subcutaneously into the post-auricular area of NOG mice. DHMEQ was administered intraperitoneally three times a week for 1 month to mice at doses of 12 mg/kg, beginning on either day 0 or day 5 when tumors were palpable. The control mice were inoculated RPMI 1640 (200 μl). Mice were sacrificed at 1-month follow-up period after inoculation. Tumor tissues were fixed with Streck Tissue Fixative (STF) and processed to paraffin wax-embedded sections for staining with hematoxylin and eosin (HE), as described.[18]

Statistical Analysis

Differences between mean values were assessed by two-tailed *t*-test. A *P*-value <0.05 was considered to be statistically significant.

RESULTS

Topoisomerase Inhibitors Induce Transient NF-κB Activation in H-RS Cell Lines Independent of IκBα Mutations

We first examined effects of topoisomerase inhibitors on the levels of NF-κB activity in H-RS cell lines without IκBα mutation (L540 and HDLM2) as well as in H-RS cells with IκBα mutations and lacking wild-type IκBα (KMH2 and L428). Treatment by SN-38, daunorubicin and etoposide further induced transient NF-κB activation, which peaked at 1 or 2 h after treatment in L540 without IκBα mutations (Figure 1a top). HDLM2, which also lacks IκBα mutation, showed a similar result (data not shown). Surprisingly, NF-κB induction, which peaked later at 4 or 5 h, was observed in H-RS cell line KMH2 bearing IκBα mutations (Figure 1a bottom). L428 bearing IκBα mutations showed transient NF-κB activation, which peaked at 1 h after treatment (data not shown). Supershift analyses using nuclear extracts prepared from H-RS cell lines at the time point of maximal NF-κB induction revealed that NF-κB includes p50 and p65. The representative results of KMH2 cells are shown in Figure 1b. Next we examined whether NF-κB induction by topoisomerase inhibitors in H-RS cell lines is mediated by IKK activation. *In vitro* kinase assay clearly showed transient activation of IKK after SN-38 treatment in both L540 and KMH2 cells (Figure 1c). These results indicate that transient NF-κB induction, which is induced independent of IκBα mutations by topoisomerase inhibitors is mediated by activation of the IKK pathway and not only constitutive, but also inducible NF-κB is a potential molecular target for treatment of HL.

Involvement of IκBβ in the Topoisomerase Inhibitor-Mediated Induction of NF-κB in H-RS Cells with IκBα Mutations

Previous reports indicated the functional redundancy and similar kinetics of IκBα and IκBβ.[19] Therefore, we examined the involvement of IκBβ in the topoisomerase inhibitor-mediated induction of NF-κB in H-RS cells with IκBα mutations and lacking IκBα. To address this point, we examined the binding of p65 and p50 with IκBβ, and the degradation and phosphorylation of IκBβ after SN-38 treatment. Previous reports indicated that like IκBα, IκBβ is also regulated by the phosphorylation of serine residues near the N terminus.[20] We used anti-phosphoserine antibody to detect phosphorylation of IκBβ. We also examined by confocal microscopy the distribution of activated NF-κB p65 and IκBβ after SN-38 treatment.

Both p65 and p50 were immunoprecipitated along with IκBβ in L428 cells (Figure 2a). In L428 cells, decreased expression of IκBβ was observed from 0.5 to 1 h after SN-38 treatment (Figure 2b). The decreased expression of IκBβ was preceded by phosphorylation of IκBβ (Figure 2c). Stimulation of L428 with SN-38 induced NF-κB activity, which peaked at 1 h (Figure 2d). Analysis by confocal microscopy revealed that active p65 NF-κB, which showed diffuse distribution before treatment, was concentrated in the nucleus 1 h after SN-38 treatment and was redistributed to the cytoplasm 2 h after SN-38 treatment (Figure 2e, top panels). IκBβ decreased the expression 1 h after SN-38 treatment (Figure 2e, bottom panels). These results indicate that IκBβ is involved in the topoisomerase inhibitor-mediated induction of NF-κB in H-RS cells lacking wild-type IκBα.

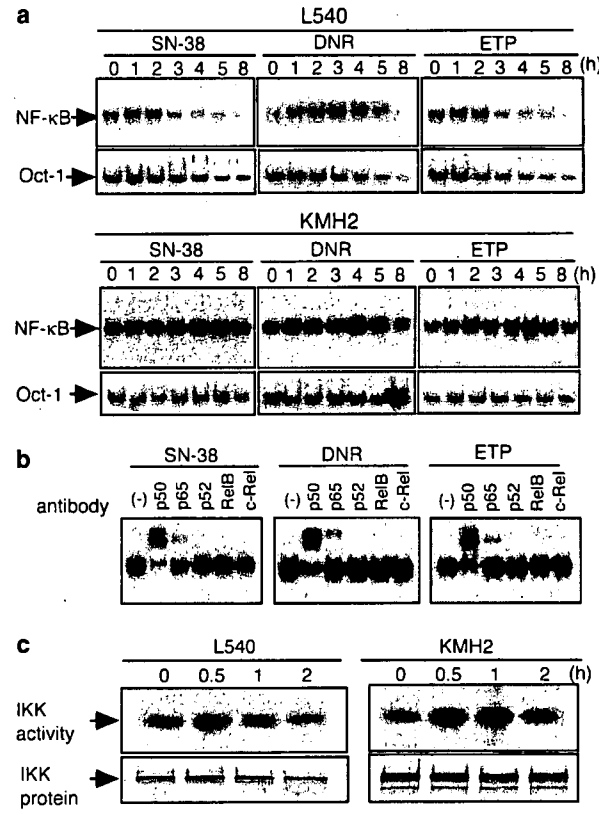

Figure 1 Treatment by topoisomerase inhibitors further induces NF-κB activity via IKK in H-RS cell lines with or without IκBα mutations. (**a**) The effect of SN-38, daunorubicin and etoposide on NF-κB activity of H-RS cells with or without IκBα mutations. H-RS cell lines; L540 cells without IκBα mutations or KMH2 cells with IκBα mutations were treated with 100 ng/ml of SN-38, 2 μM daunorubicin or 50 μM etoposide for indicated hours. Nuclear extracts (1 μg) were examined for NF-κB-binding activity by EMSA with radiolabeled NF-κB specific probe. Topoisomerase inhibitors used are indicated above. DNR, daunorubicin; ETP, etoposide. Lower panels show results of EMSA with a control probe, Oct-1. (**b**) Analysis of NF-κB subcomponent after treatment with topoisomerase inhibitors by supershift assay. KMH2 cells were treated with topoisomerase inhibitors for 5 h and harvested.Two micrograms of nuclear extracts were subjected to analysis. Antibodies used are indicated above. (**c**) *In vitro* kinase assay of H-RS cell lines with or without IκBα mutations. L540 cell or KMH2 cells treated with 100 ng/ml of SN-38 for indicated hours were immunoprecipitated by anti-IKK antibody and subjected to *in vitro* kinase assay using IκBα as substrate. Phosphorylation of IκBα by IKK, which represents IKK activity, is shown in the upper panels. Immunoblot of immunoprecipitates by anti-IKK antibody in lower panels shows an equal amount of IKK was used in each reaction.

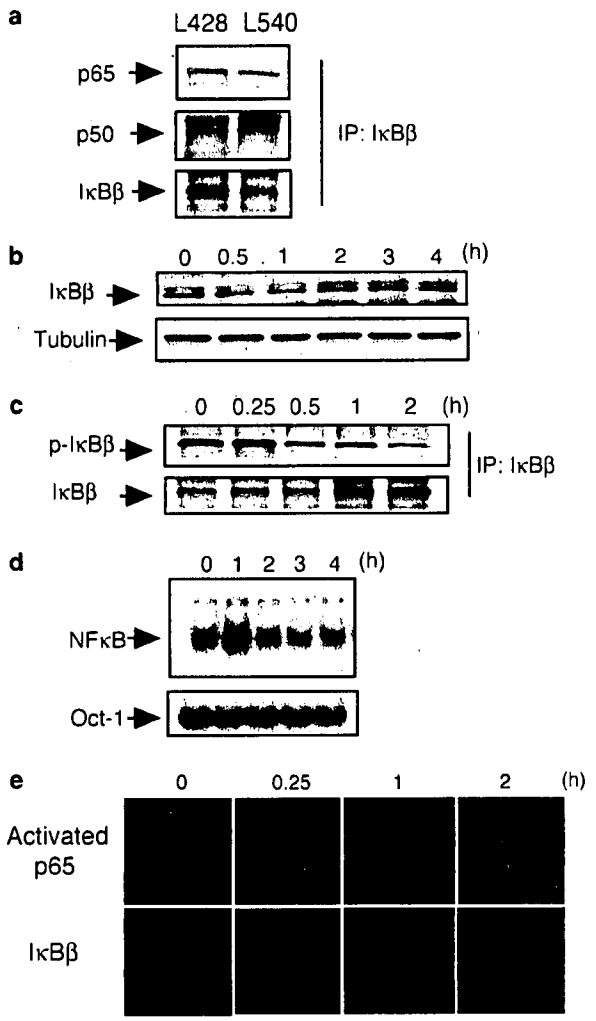

Figure 2 Topoisomerase inhibitor-mediated induction of NF-κB is mediated by the phosphorylation and degradation of IκBβ in H-RS cells with IκBα mutations. (**a**) Coimmunoprecipitation analysis of NF-κB p50 and p65 with IκBβ. Immunoprecipitates of anti-IκBβ antibody were blotted with anti-NF-κB p50 or p65 antibodies (upper panels). Immunoprecipitates were blotted with anti-IκBβ antibody (bottom panel). IP, immunoprecipitation. (**b**) Expression level of IκBβ protein in L428 cells after treatment with topoisomerase inhibitor. Whole cell lysates of L428 treated with SN-38 for the indicated number of hours were blotted with anti-IκBβ antibody (upper panel) or anti-α tubulin antibody (bottom panel). (**c**) Phosphorylation of IκBβ protein in L428 cells after treatment with topoisomerase inhibitor. L428 cells were treated with 100 ng/ml of SN-38 for the indicated number of hours. Immunoprecipitates of anti-IκBβ antibody were blotted with anti-phosphoserine antibody (upper panel) or anti-IκBβ antibody (bottom panel). (**d**) The effect of SN-38 on NF-κB activity in L428 cells. L428 cells were treated with 100 ng/ml of SN-38 for the indicated number of hours. Nuclear extracts (1 μg) were examined for NF-κB-binding activity by EMSA with radiolabeled NF-κB-specific probe. (**e**) Localization of activated NF-κB p65 and IκBβ after treatment with topoisomerase inhibitor. L428 cells were treated with 100 ng/ml of SN-38 for the indicated number of hours. Confocal immunofluorescence microscopic analysis was performed on cytospin samples stained with antibodies against activated NF-κB p65 and IκBβ.

DHMEQ Reduces Cell Growth and Induces Apoptosis of H-RS Cells Through Inhibition of Constitutive NF-κB Activity

We next examined the effects of DHMEQ on constitutive NF-κB activity in H-RS cell lines. Treatment with DHMEQ at a concentration of 10 μg/ml abrogated constitutive NF-κB-binding activity in these cell lines (Figure 3a). Inhibition of constitutive NF-κB activity by DHMEQ was observed in all H-RS cell lines examined irrespective of presence (L428 and KMH2) or absence (L540 and HDLM2) of IκBα mutations. Analysis by confocal microscopy revealed accumulation of active form of NF-κB p65 in the cytoplasm after DHMEQ treatment in KMH2 and L540, indicating action of DHMEQ at the level of translocation of NF-κB into the nucleus (Figure 3b). Time-course studies showed that DHMEQ almost completely abrogated NF-κB binding activity at 1 hour after DHMEQ treatment and thereafter for 16 h (Figure 3c). The supershift assays revealed that the affected NF-κB components include p50 and p65 as reported previously[9] (Figure 3d).

We next examined the effect of DHMEQ on viability of H-RS cell lines (Figure 4). Results of MTT assays showed that DHMEQ treatment reduced cell viability of all four H-RS-derived cell lines in a dose-dependent manner, whereas it did not show a significant effect on the viability of PBMC even at higher concentrations (Figure 4a). Furthermore, we examined whether DHMEQ induces apoptosis of H-RS cell lines by analyzing Annexin V reactivity and nuclear fragmentation. Based on the results obtained from MTT assays, L428 and KMH2 cells were treated with 20 μg/ml, and L540 and HDLM2 cells were treated with 10 μg/ml of DHMEQ. Flow cytometric analysis showed a significant increase in the number of Annexin V-positive cells after DHMEQ treatment in H-RS cell lines, but not in PBMC (Figure 4b). Hoechst 33342 staining showed fragmentation and condensation of the nucleus of H-RS cell lines, suggesting induction of apoptosis in these cells, but not in normal PBMC (Figure 4c).

Taken together, these results indicate that DHMEQ selectively targets constitutive NF-κB activity in H-RS cells and induces apoptosis of these cells independent of IκBα mutations.

DHMEQ-Induced Apoptosis Involves Activation of Caspases 3, 8 and 9

To examine whether induction of apoptosis upon inhibition of constitutive NF-κB activity in H-RS cells by DHMEQ is caused by the activation of the caspase pathway, we first studied activation of caspase 3 by immunoblot analysis. Results clearly showed cleavage of caspase 3, suggesting DHMEQ-induced apoptosis is associated with activation of the caspase pathway (Figure 5a, top panel). To differentiate the membranous and mitochondrial pathways, we next examined activation of caspase 8 and 9 that are upstream of caspase 3 by immunoblot analysis. DHMEQ-treated H-RS cells showed activation of both caspases 8 and 9 (Figure 5a

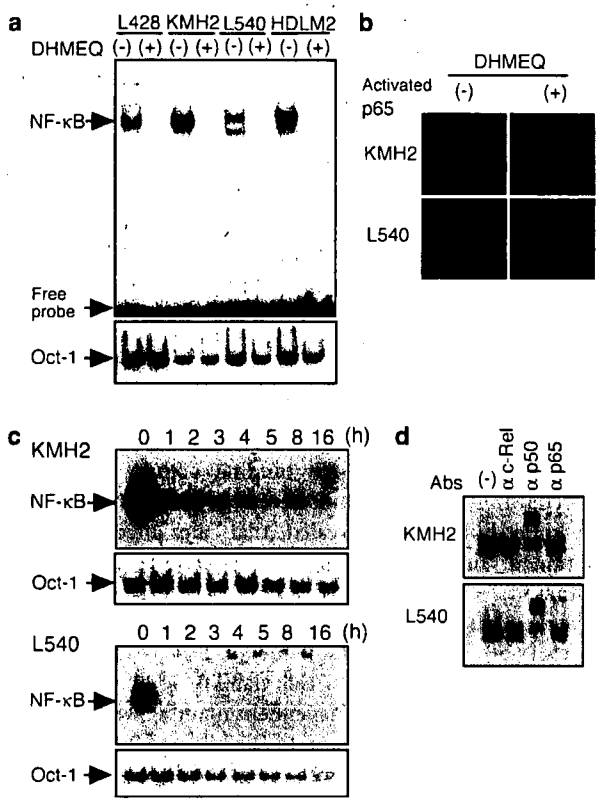

Figure 3 DHMEQ suppresses constitutive NF-κB activity in H-RS cell lines. (**a**) Inhibition of constitutive NF-κB-binding activity in H-RS cell lines. H-RS cell lines, L428, KMH2, L540 and HDLM2, were treated with (+) or without (−) 10 μg/ml of DHMEQ for 7 h. Nuclear extracts (2 μg) were examined for NF-κB binding activity by EMSA with a radiolabeled NF-κB specific probe. The upper panel shows inhibition of NF-κB-binding activity by DHMEQ. The lower panel shows results of EMSA with a control probe, Oct-1. The position of shifted bands corresponding to NF-κB and free probes are indicated on the left. (**b**) Accumulation of active NF-κB p65 in the cytoplasm after DHMEQ treatment. KMH2 and L540 cells were treated with or without 10 μg/ml of DHMEQ for 6 h. Confocal immunofluorescence microscopic analysis was carried out on cytospin samples stained with antibody against active NF-κB p65. (**c**) Time-course studies of NF-κB inhibition by DHMEQ. KMH2 and L540 cells were treated with 10 μg/ml of DHMEQ for indicated hours. Nuclear extracts (2 μg) were examined for NF-κB-binding activity by EMSA with a radiolabeled NF-κB-specific probe. EMSA with Oct-1 served as control. (**d**) NF-κB subcomponent analysis in H-RS cell lines. Subcomponents of NF-κB constitutively activated in H-RS cell lines were determined by supershift analysis. Nuclear extracts (2 μg) of untreated H-RS cell lines were subjected to supershift analysis with antibodies specific for c-Rel, NF-κB p50 and NF-κB p65. Cell lines used are indicated on the left.

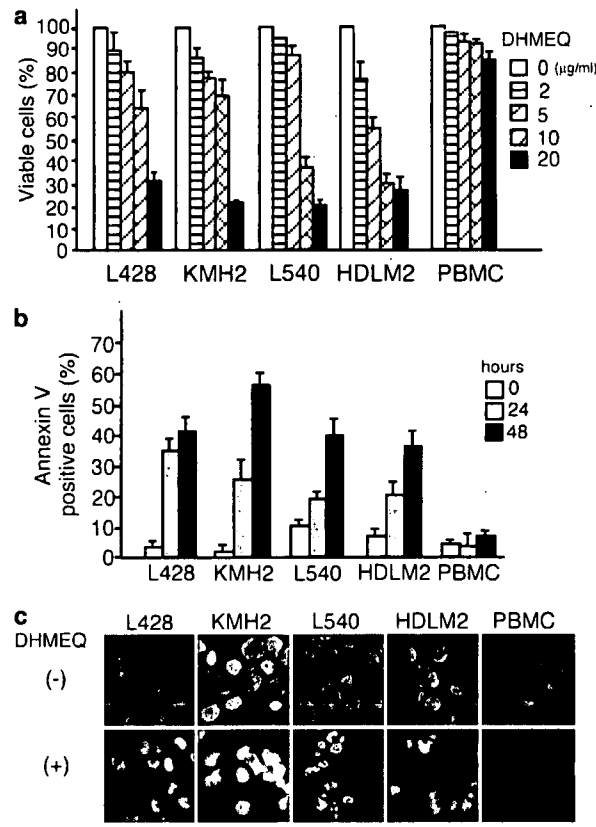

Figure 4. DHMEQ induces apoptosis of H-RS cell lines. (**a**) Dose-dependent reduction of cell viabilities of H-RS cell lines treated with DHMEQ. H-RS cell lines; L428, KMH2, L540 and HDLM2 as well as PBMC were treated with indicated concentrations of DHMEQ for 48 h. Cell viabilities were determined by MTT assay. Data represent the mean ± s.d. of three independent experiments. (**b**) Flow cytometric analysis of Annexin V-reactive cells. L428 and KMH2 cells were treated with 20 μg/ml of DHMEQ for indicated hours. L540 and HDLM2 cells were treated with 10 μg/ml of DHMEQ. PBMC were treated with 20 μg/ml of DHMEQ. After labeling with FITC-conjugated Annexin V, cells were analyzed by flow cytometry. Data represent the mean ± s.d. of three independent experiments. (**c**) Nuclear fragmentation of cells treated with DHMEQ. Cells were treated with the same concentration of DHMEQ used in the detection of Annexin V reactive cells for 48 h and stained with 10 μM Hoechst 33342. Cells used are indicated above.

second and third panels). To confirm this, we next studied whether inhibitors of caspase 3, 8 and 9 can inhibit DHMEQ-induced apoptosis. The results demonstrated significant alleviation of apoptosis in the cells treated by these inhibitors, although inhibition of apoptosis was not complete (Figure 5b). These results suggested that the apoptosis induced by DHMEQ is mediated by both membranous and mitochondrial caspase pathways.

Recent reports indicate frequent expression of anti-apoptotic genes Bcl-xL and c-FLIP whose constitutive induction are critically involved in anti-apoptotic activity in H-RS cells.[21–24] Bcl-xL and c-FLIP antagonize mitochondrial and membranous caspase activities.[25] We next examined changes in their expression upon DHMEQ treatment by Northern blotting and immunohistochemistry. The result confirmed downregulation of Bcl-xL and c-FLIP mRNAs (Figure 5c). We also examined the protein expression of Bcl-xL and c-FLIP by immunofluorescence confocal microscopy. The results clearly showed downregulation of expression of these proteins (Figure 5d). Taken together, these data confirmed that DHMEQ induced apoptosis of H-RS cell lines is

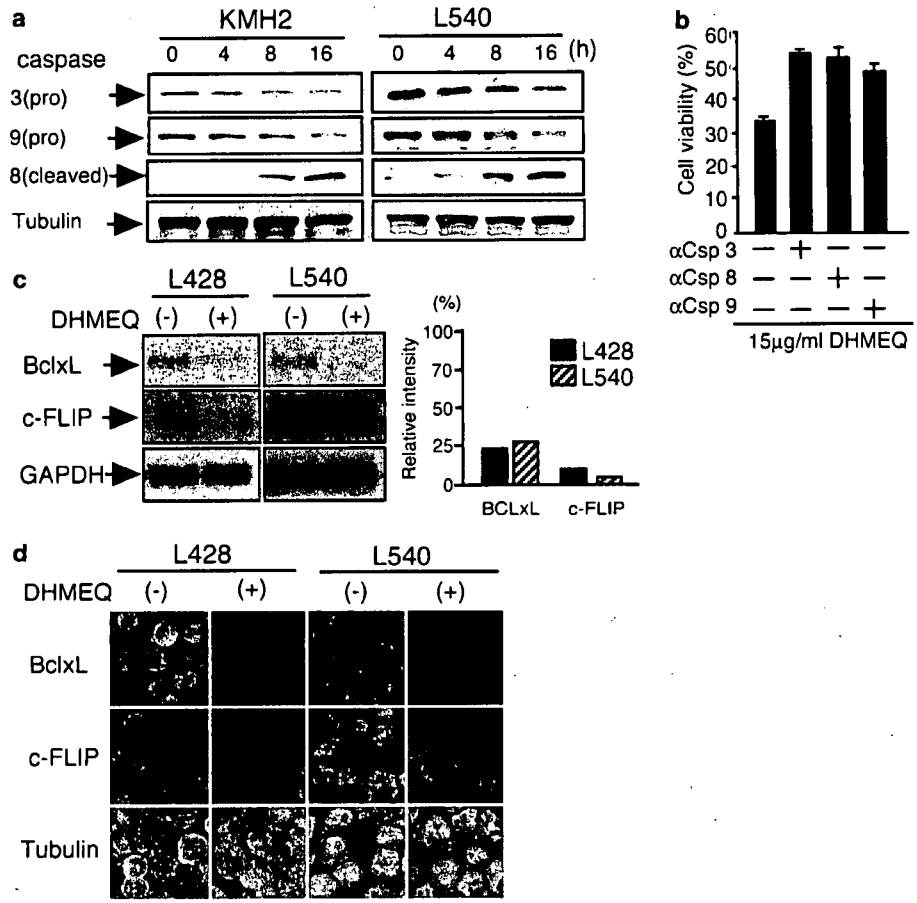

Figure 5 DHMEQ-induced apoptosis of H-RS cell lines involves activation of membranous and mitochondrial caspase pathways and downregulation of c-FLIP and Bcl-xL. (**a**) Immunoblot analyses of caspase -3, -8 and -9. L540 cells were treated with 10 μg/ml of DHMEQ and KMH2 cells were treated of 20 μg/ml with DHMEQ for indicated hours. 30 μg of whole cell lysates were subjected to the analysis. (**b**) Inhibition of DHMEQ induced apoptosis by blockade of caspase-3, -8 and -9 activities in KMH2 cells. Before the incubation with 15 μg/ml of DHMEQ, KMH2 cells were treated with 50 μM of caspase 3 inhibitor z-DEVD-FMK, caspase 8 inhibitor z-IETD-FMK or caspase 9 inhibitor z-LEHD-FMK. After 12 h of treatment with DHMEQ, cells were analyzed by MTT assay. α-Csp, anti-caspase. (**c**) The expression of Bcl-xL and c-FLIP mRNA. L428 and L540 cells were treated with or without 10 μg/ml of DHMEQ for 16 h. The expression of Bcl-xL and c-FLIP was examined by Northern blot analysis, using RT-PCR amplified fragments as probes. Two microgramof poly (A)-selected RNA were subjected to the analysis. Results of Northern blot analyses are shown on the left. Expression of GAPDH served as a control. Quantification of relative levels of expression is shown on the right. GAPDH signals were measured by densitometry and the values were used to normalize the levels of densitometric quantification of Bcl-xL and c-FLIP mRNA expression in L428 and L540 cells. The relative expression levels of treated samples are expressed as percentages of those of untreated ones, which are set to 100%. (**d**) Expression of Bcl-xL and c-FLIP proteins involved in anti-apoptosis. L428 and L540 cells were treated with or without 10 μg/ml of DHMEQ for 16 h. Cells were spun by centrifugation onto glass coverslips and stained with antibodies specific for Bcl-xL and c-FLIP and observed with fluorescence confocal microscopy. Expression of α-tubulin served as control.

mediated via mitochondrial and membranous pathway, which are accompanied by downregulation of Bcl-xL and c-FLIP.

DHMEQ Shows a Potent Inhibitory Effect on the Growth of H-RS Cells in NOG Mice Model

As the above results suggested potential efficacy of DHMEQ for the treatment of patients with HL by inhibiting constitutive NF-κB activity, we next examined whether DHMEQ treatment can suppress growth of xenografted H-RS cells in the NOG mice model. As expected, DHMEQ treatment resulted in reduction of the tumor mass at 1 month after inoculation (Figure 6a). A significant decrease in the size and weight of tumors in mice treated with DHMEQ was demonstrated when compared with controls at 1 month (Figure 6b). DHMEQ also inhibited the size and growth of tumors established by inoculation of L540 and KMH2 cells, indicating that the action of DHMEQ is independent of lack of wild-type IκBα as is expected by experiments *in vitro* (Figure 6c and d). DHMEQ at this treatment dosage (12 mg/kg of DHMEQ, three times a week for 1 month) is well tolerated without adverse findings such as weight loss or cachexia of treated mice. As expected, microscopic analysis of tumors revealed apoptotic cells in specimens from

DHMEQ-treated mice (Figure 6e). These results suggest that DHMEQ contributes to the reduction of HL tumors independent of lack of IκBα in mice model.

DHMEQ Enhances Anti-Tumor Effect of Topoisomerase Inhibitors by Blocking Inducible NF-κB in H-RS Cells

We next examined the effects of DHMEQ on NF-κB activity induced by topoisomerase inhibitors in KMH2 cells. Treatment by DHMEQ almost completely abrogated both constitutive and inducible NF-κB activities (Figure 7a). Analysis by confocal microscopy revealed accumulation of active form of NF-κB p65 in the cytoplasm of KMH2 cells treated with SN-38 and DHMEQ, supporting the notion that DHMEQ inhibits these NF-κB at the level of translocation into the nucleus (Figure 7b).

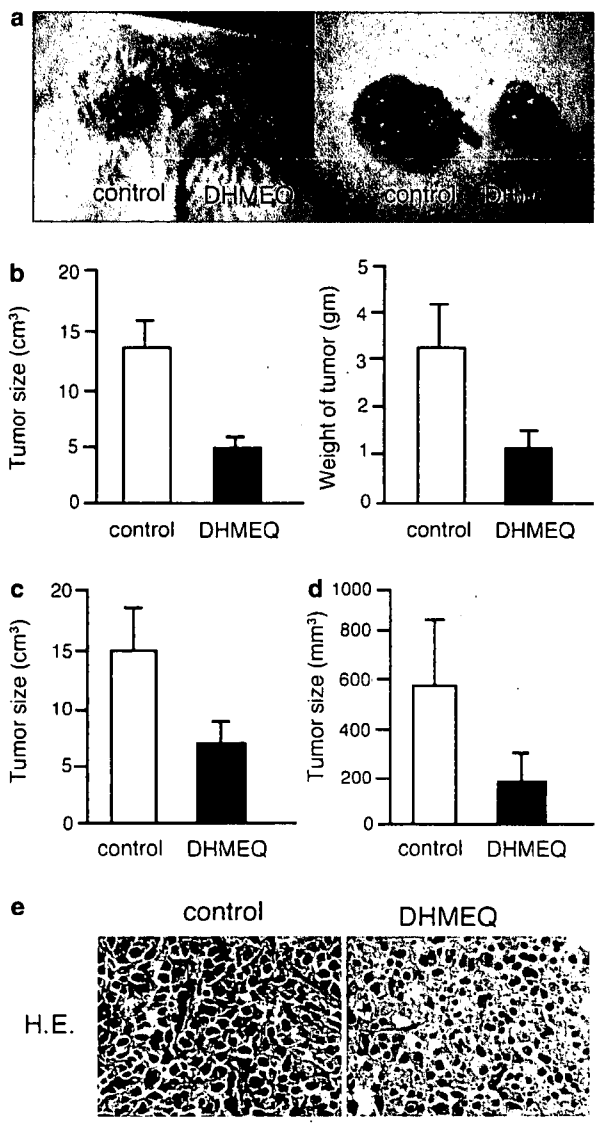

We next examined whether topoisomerase inhibitors and DHMEQ show enhanced anti-tumor effects in H-RS cell lines. We incubated KMH2 cells with sublethal concentrations of SN-38 with or without 10 μg/ml of DHMEQ for 48 h. The viability of the cells was measured by MTT assay. Combination of DHMEQ and SN-38 showed enhanced effect in the reduction of cell viability of KMH2 cells (Figure 7c left panel). Other topoisomerase inhibitors, daunorubicin and etoposide also revealed almost the same effects (Figure 7c middle and right panel).

To explore whether the combined effects result in enhanced induction of apoptosis, we examined expression of Annexin V, a marker for the early stage of apoptosis, and nuclear fragmentation of KMH2 cells. In each combination with one of three topoisomerase inhibitors, DHMEQ treatment enhanced Annexin V staining (Figure 7d) and fragmentation or condensation of the nuclei (Figure 7e). DHMEQ also enhanced SN-38-induced activation of caspase 3 in L428 cells (Figure 7f). These observations indicate that blockade of inducible NF-κB by DHMEQ enhances the anti-tumor effects of topoisomerase inhibitors in H-RS cells.

DISCUSSION

In this study, we showed that although the NF-κB level of H-RS cell is very high, topoisomerase inhibitors further stimulated NF-κB activity through IKK activation in not only H-RS cell lines with wild-type IκBα, but also H-RS cell lines with defective IκBα. We presented the supportive evidence that IκBβ is involved in NF-κB induction in H-RS cells. We also showed that a new NF-κB inhibitor, DHMEQ-enhanced cytotoxicity of topoisomerase inhibitors by inhibiting inducible NF-κB, independent of the presence or absence of IκBα mutations in H-RS cell lines. The results suggest that constitutive and inducible NF-κB are appropriate molecular targets for the treatment of HL, and DHMEQ is a suitable compound to target these NF-κB.

Figure 6 Effects of DHMEQ on H-RS cell lines inoculated in NOG mice. A total of 1×10^7 cells were inoculated in the post-auricular region of NOG mice. For the treatment group, 12 mg/kg of DHMEQ was administered intraperitoneally three times a week for 1 month, beginning on either day 0 or day 5 when tumors were palpable and established. The control mice received RPMI 1640 (200 μl) simultaneously. (**a**) Gross appearance of the mice with (right) or without (left) DHMEQ treatment. Macroscopic images of subcutaneous tumors formed by L540 and those resected from mice with (right) or without (left) DHMEQ treatment, which began on day 0. (**b**) Size and weight of the resected tumors were measured and represented as bar graphs. Data represent the mean ± s.d. from six mice. (**c** and **d**) Effects of DHMEQ on established tumors. L540 cells (**c**) and KMH2 cells (**d**) were used for the experiments. Size of tumors was measured and represented as bar graphs. Data represent the mean ± s.d. from four mice. (**e**) Growth inhibitory effect of DHMEQ on L540 cells is accompanied by apoptosis. Microscopic images of HE-stained tumor tissues of mice with or without DHMEQ treatment (right and left, respectively) revealed apoptotic cells in DHMEQ-treated mice.

Activation of IKK and IκBα upon NF-κB induction by topoisomerase inhibitors has been well-documented.[12,14] Topoisomerase inhibitors are thought to mobilize a pre-existing signaling pathway that starts from the nucleus at the level of DNA strand breaks to end up in the cytosol at the IKK complex. Several candidate molecules such as ATM

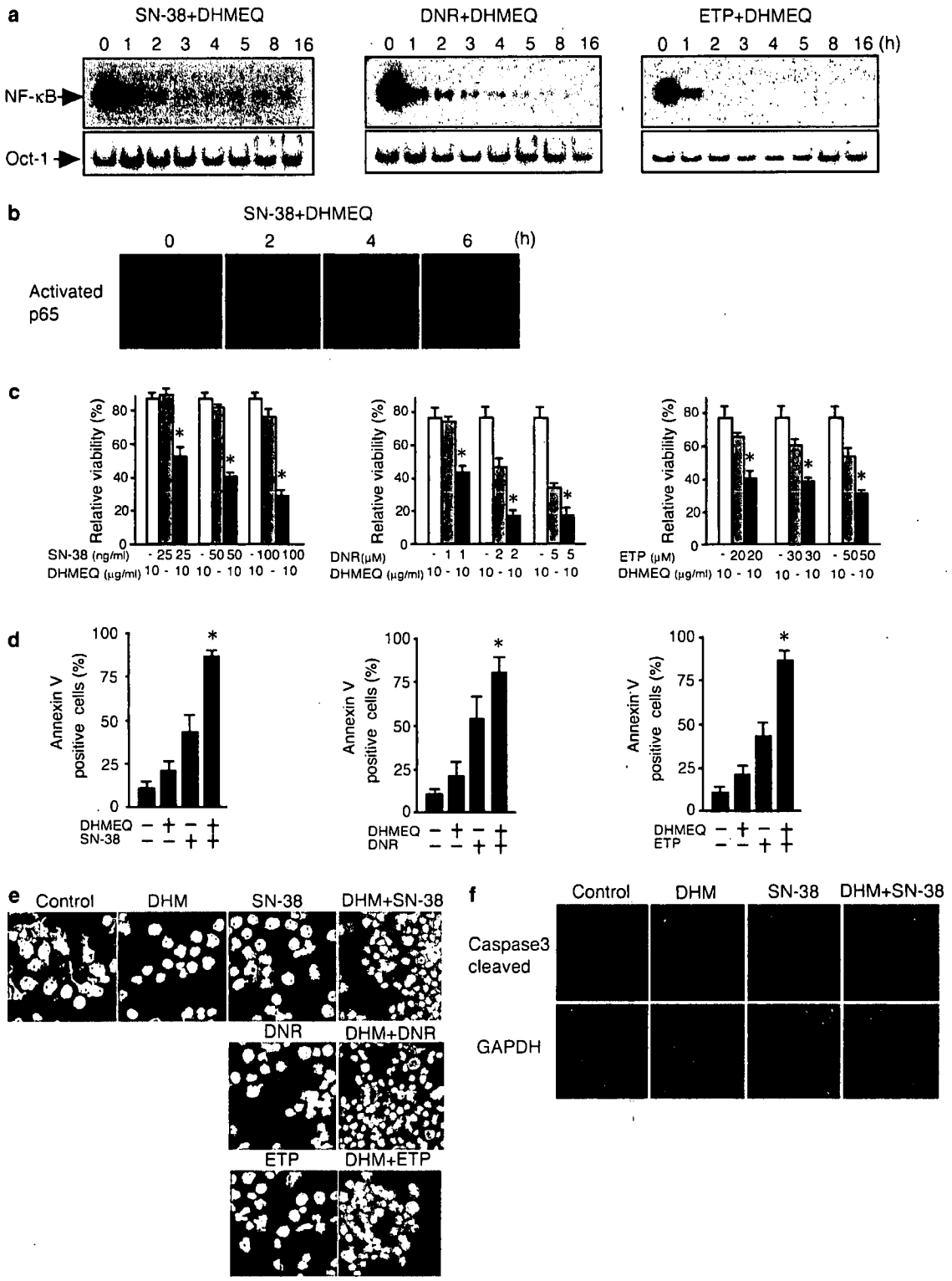

and DNA-PK involved in this step have been reported.[26,27] A previous study excluded involvement of an autocrine NF-κB activator synthesized by stimulation of topoisomerase inhibitors.[12] Transient activation of IKK and NF-κB by topoisomerase inhibitors in H-RS cell lines indicates that similar kind of activation pathway also operates in H-RS cells having strong and constitutive NF-κB activity.

About 10–20% of H-RS cells are reported to harbor hetero- or homo-genetic alteration of IκBα genes resulting in the production of defective IκBα lacking C-terminal domain unable to bind with NF-κB. Lack of wild-type IκBα by IκBα mutations has been reported to one of the causes of constitutive NF-κB activation in H-RS cells.[3–7] If IκBα is the only molecule that regulates NF-κB in H-RS cells, lack of wild-type IκBα may cause deregulated activation of NF-κB independent of upstream IKK signals. However, IKK-mediated induction of NF-κB by topoisomerase inhibitors in H-RS cell lines lacking wild-type IκBα suggests the existence of other molecules that regulate NF-κB activity by substitution for IκBα. Our previous result that adenovirus-mediated transduction of decoy CD30 lacking the cytoplasmic domain inhibits NF-κB activity and the recent report that proteasome inhibitor PS341 induces apoptosis in H-RS cell lines lacking wild-type IκBα, support the above hypothesis.[8,28] The results in this study indicate that IκBβ is involved in NF-κB activation in H-RS cells and IκBβ substitutes for IκBα in H-RS cells lacking wild-type IκBα. Functional redundancy and similar kinetics of activities of IκBα and IκBβ reported previously also support the above notion.[19]

The results obtained in this study suggest that not only constitutive, but also inducible NF-κB activities are good molecular targets of HL treatment. The results confirmed that topoisomerase inhibitors, SN-38, daunorubicin and etoposide can further induce transient NF-κB activation in addition to the basal strong and constitutive NF-κB activity in H-RS cell lines. Previous studies showed that stimulation of H-RS cell lines by TNF family members; CD40L or TNF cannot enhance NF-κB activity.[5,6] These observations indicate that in H-RS cells, signals from TNF receptor family members to IKK complex, which are mediated by TRAF proteins, are fully active, whereas IKK complex is still responsible for TRAF-independent stimulation. The demonstration that DHMEQ enhanced effects of topoisomerase inhibitors by blocking inducible NF-κB, suggests that inducible NF-κB blunts the effects of topoisomerase inhibitors in H-RS cells and DHMEQ can restore this effect.

Blockade of NF-κB is evident at 1 h and thereafter (Figure 3c), apoptosis induction was at a relatively late event after DHMEQ treatment (Figure 4b). Therefore, induction of apoptosis in H-RS cells by DHMEQ may be indirect and mediated by altered levels of gene expression. As inhibition of constitutive NF-κB activation is sufficient to trigger apoptosis of H-RS cells without stimulation of death receptor or cytotoxic agents, survival of H-RS cells appears to depend on a balance between anti-apoptotic and pro-apoptotic activities. In support of this notion, the present study confirmed the downregulation of c-FLIP and Bcl-xL, which are reported to be frequently expressed in H-RS cells upon blocking of NF-κB activity[21–24] (Figure 5c and d).

Prompt and specific action of DHMEQ suggests that DHMEQ is a suitable compound to target NF-κB in H-RS cells. Recent studies in other laboratories using gliotoxin, MG132, arcenic and PS341 also suggest that low-molecular-weight compounds have a potential to inhibit NF-κB in H-RS cells. However, their specificity for the NF-κB pathway appears to be relatively low when compared with that of DHMEQ.[28–30] The target of DHMEQ resides downstream of targets of gliotoxin, MG132, arcenic and PS341. Furthermore, inhibition of NF-κB by gliotoxin, MG132, and PS341 is only one of the results of their activities as proteasome inhibitors.[28,29] Arsenic also alters a variety of enzymatic activities because of reactivity with sulfhydryl groups.[30]

The unique properties of DHMEQ appear to minimize adverse effects on normal cells. Notably, PBMC are resistant to apoptosis by DHMEQ treatment, although the mechanism is not currently understood. Results of our *in vivo* model suggest that DHMEQ may be minimally less toxic at effective doses. Treatment of mice with DHMEQ three times a week

Figure 7 DHMEQ abrogates inducible NF-κB and enhances anti-tumor effect of topoisomerase inhibitors in H-RS cell lines. (**a**) Inhibition of topoisomerase inhibitors-mediated NF-κB induction by DHMEQ. KMH2 cells were exposed to 100 ng/ml of SN-38, 2 μM daunorubicin or 50 μM etoposide in combination with 10 μg/ml of DHMEQ for indicated hours. Two microgram of nuclear extracts were examined for NF-κB-binding activity by EMSA using NF-κB probe. Lower panels show results of EMSA with a control probe, Oct-1. DNR, daunorubicin; ETP, etoposide. (**b**) Accumulation of active NF-κB p65 after DHMEQ treatment. KMH2 cells were exposed to 100 ng/ml of SN-38 in combination with 10 μg/ml of DHMEQ for indicated hours. Confocal immunofluorescence microscopic analysis was carried out on cytospin samples stained with antibody against active NF-κB p65. (**c**) Effect of DHMEQ on viability of H-RS cells treated by topoisomerase inhibitors. KMH2 cells were treated with indicated concentrations of topoisomerase inhibitors with or without 10 μg/ml of DHMEQ. Forty-eight hours after treatment, cell viability was measured by MTT assay and the relative viability was determined. MTT values of DMSO-treated cells were set to 100%. Data present the mean ± s.d. of three independent experiments. $^*P < 0.05$, compared with SN-38, DNR or ETP alone. (**d**) Analysis of Annexin V-reactive cells. KMH2 cells were treated with 10 μg/ml of DHMEQ with or without topoisomerase inhibitors for 24 h. Cells were stained by FITC-conjugated Annexin V and analyzed by flow cytometry. Data present the mean ± s.d. of three independent experiments. Concentration of the agents was SN-38; 100 ng/ml, daunorubicine; 2 μM and etoposide; 50 μM. $^*P < 0.05$, compared with SN-38, DNR or ETP alone. (**e**) Nuclear fragmentation. KMH2 cells were treated with topoisomerase inhibitors with or without 10 μg/ml of DHMEQ for 24 h. After treatment, KMH2 cells were harvested and subjected to staining by Hoechst 33342. Concentration of the agents was the same as in flow cytometric analysis of Annexin V-reactive cells DHM, DHMEQ. (**f**) Activation of caspase-3. L428 cells were treated with 100 ng/ml of SN-38 with or without 10 μg/ml of DHMEQ for 24 h. Cells were spun onto slide glass and stained with antibody for cleaved caspase-3 and analyzed by confocal microscopy. Staining by GAPDH served as a control.

showed significant anti-tumor activity. DHMEQ treatment did not show significant systemic toxicity such as body weight loss in these experiments. The dose of DHMEQ used in these experiments (12 mg/kg) is far less than LD50 of DHMEQ that is 180 mg/kg (unpublished observation). Therefore, DHMEQ may be more suitable for NF-κB inhibition in H-RS cells.

In conclusion, both constitutive and inducible NF-κB are potential molecular targets to treat HL independent of the presence of IκBα mutations. NF-κB inhibitor DHMEQ is a suitable candidate to translate this strategy into clinical medicine. The results also indicate that IκBβ is involved in NF-κB activation in H-RS cells and IκBβ substitutes for IκBα in H-RS cells lacking wild-type IκBα.

ACKNOWLEDGEMENT

We thank Y Sato, National Institute of Infectious Diseases for technical assistance. Supported in part by Grants-in-Aid for Scientific Research from Japanese Society for Promotion of Science to R Horie and T Watanabe and Integrative Research Program of the Graduate School of Medical Sciences, Kitasato University to R Horie. Also supported in part by grants from the Ministry of Education, Science and Culture, Ministry of Health, Labor and Welfare and Human Health Science of Japan to N Yamamoto. Dr Kadin is supported by NIH Grant P50-CA-93683-05.

1. Diehl V, Thomas RK, Re D. Part II: Hodgkin's lymphoma—diagnosis and treatment. Lancet Oncol 2004;5:19–26.
2. Griffin J. The biology of signal transduction inhibition: basic science to novel therapies. Semin Oncol 2001;28:3–8.
3. Emmerich F, Meiser M, Hummel M, *et al.* Overexpression of I kappa B alpha without inhibition of NF-kappaB activity and mutations in the I kappa B alpha gene in Reed-Sternberg cells. Blood 1999;94:3129–3134.
4. Jungnickel B, Staratschek-Jox A, Brauninger A, *et al.* Clonal deleterious mutations in the IkappaBalpha gene in the malignant cells in Hodgkin's lymphoma. J Exp Med 2000;191:395–402.
5. Krappmann D, Emmerich F, Kordes U, *et al.* Molecular mechanisms of constitutive NF-kappaB/Rel activation in Hodgkin/Reed-Sternberg cells. Oncogene 1999;18:943–953.
6. Wood KM, Roff M, Hay RT. Defective IkappaBalpha in Hodgkin cell lines with constitutively active NF-kappaB. Oncogene 1998;16:2131–2139.
7. Cabannes E, Khan G, Aillet F, *et al.* Mutations in the IkBa gene in Hodgkin's disease suggest a tumour suppressor role for IkappaBalpha. Oncogene 1999;18:3063–3070.
8. Horie R, Watanabe T, Morishita Y, *et al.* Ligand-independent signaling by overexpressed CD30 drives NF-kappaB activation in Hodgkin/Reed-Sternberg cells. Oncogene 2002;21:2493–2503.
9. Bargou RC, Leng C, Krappmann D, *et al.* High-level nuclear NF-kappa B and Oct-2 is a common feature of cultured Hodgkin/Reed-Sternberg cells. Blood 1996;87:4340–4347.
10. Bargou RC, Emmerich F, Krappmann D, *et al.* Constitutive nuclear factor-kappaB-RelA activation is required for proliferation and survival of Hodgkin's disease tumor cells. J Clin Invest 1997;100:2961–2969.
11. Mayo MW, Baldwin AS. The transcription factor NF-kappaB: control of oncogenesis and cancer therapy resistance. Biochim Biophys Acta 2000;1470:M55–M62.
12. Bottero V, Busuttil V, Loubat A, *et al.* Activation of nuclear factor kappaB through the IKK complex by the topoisomerase poisons SN38 and doxorubicin: a brake to apoptosis in HeLa human carcinoma cells. Cancer Res 2001;61:7785–7791.
13. Wang CY, Cusack Jr JC, Liu R, *et al.* Control of inducible chemoresistance: enhanced anti-tumor therapy through increased apoptosis by inhibition of NF-kappaB. Nat Med 1999;5:412–417.
14. Cusack Jr JC, Liu R, Houston M, *et al.* Enhanced chemosensitivity to CPT-11 with proteasome inhibitor PS-341: implications for systemic nuclear factor-kappaB inhibition. Cancer Res 2001;61: 3535–3540.
15. Ariga A, Namekawa J, Matsumoto N, *et al.* Inhibition of tumor necrosis factor-alpha -induced nuclear translocation and activation of NF-kappa B by dehydroxymethylepoxyquinomicin. J Biol Chem 2002;277: 24625–24630.
16. Matsumoto N, Ariga A, To-e S, *et al.* Synthesis of NF-kappaB activation inhibitors derived from epoxyquinomicin C. Bioorg Med Chem Lett 2000;10:865–869.
17. Horie R, Watanabe M, Ishida T, *et al.* The NPM-ALK oncoprotein abrogates CD30 signaling and constitutive NF-kappaB activation in anaplastic large cell lymphoma. Cancer Cell 2004;5:353–364.
18. Dewan MZ, Watanabe M, Terashima K, *et al.* Prompt tumor formation and maintenance of constitutive NF-kappaB activity of multiple myeloma cells in NOD/SCID/gammacnull mice. Cancer Sci 2004;95:564–568.
19. Cheng JD, Ryseck RP, Attar RM, *et al.* Functional redundancy of the nuclear factor kappa B inhibitors I kappa B alpha and I kappa B beta. J Exp Med 1998;188:1055–1062.
20. Huang TT, Miyamoto S. Postrepression activation of NF-kappaB requires the amino-terminal nuclear export signal specific to IkappaBalpha. Mol Cell Biol 2001;21:4737–4747.
21. Kim LH, Nadarajah VS, Peh SC, *et al.* Expression of Bcl-2 family members and presence of Epstein-Barr virus in the regulation of cell growth and death in classical Hodgkin's lymphoma. Histopathology 2004;44:257–267.
22. Dutton A, O'Neil JD, Milner AE, *et al.* Expression of the cellular FLICE-inhibitory protein (c-FLIP) protects Hodgkin's lymphoma cells from autonomous Fas-mediated death. Proc Natl Acad Sci USA 2004;101:6611–6616.
23. Thomas RK, Kallenborn A, Wickenhauser C, *et al.* Constitutive expression of c-FLIP in Hodgkin and Reed-Sternberg cells. Am J Pathol 2002;160:1521–1528.
24. Mathas S, Lietz A, Anagnostopoulos I, *et al.* c-FLIP mediates resistance of Hodgkin/Reed-Sternberg cells to death receptor-induced apoptosis. J Exp Med 2004;199:1041–1052.
25. Debatin KM. Apoptosis pathways in cancer and cancer therapy. Cancer Immunol Immunother 2004;53:153–159.
26. Piret B, Schoonbroodt S, Piette J. The ATM protein is required for sustained activation of NF-kappaB following DNA damage. Oncogene 1999;18:2261–2271.
27. Basu S, Rosenzweig KR, Youmell M, *et al.* The DNA-dependent protein kinase participates in the activation of NF kappa B following DNA damage. Biochem Biophys Res Commun 1998;247:79–83.
28. Zheng B, Georgakis GV, Li Y, *et al.* Induction of cell cycle arrest and apoptosis by the proteasome inhibitor PS-341 in Hodgkin disease cell lines is independent of inhibitor of nuclear factor-kappaB mutations or activation of the CD30, CD40, and RANK receptors. Clin Cancer Res 2004;10:3207–3215.
29. Izban KF, Ergin M, Huang Q, *et al.* Characterization of NF-kappaB expression in Hodgkin's disease: inhibition of constitutively expressed NF-kappaB results in spontaneous caspase-independent apoptosis in Hodgkin and Reed-Sternberg cells. Mod Pathol 2001;14: 297–310.
30. Mathas S, Lietz A, Janz M, *et al.* Inhibition of NF-kappaB essentially contributes to arsenic-induced apoptosis. Blood 2003;102:1028–1034.

Whole-genome profiling of chromosomal aberrations in hepatoblastoma using high-density single-nucleotide polymorphism genotyping microarrays

Makoto Suzuki,[1,6] Motohiro Kato,[2] Chen Yuyan,[2] Junko Takita,[3] Masashi Sanada,[4] Yasuhito Nannya,[4] Go Yamamoto,[4] Atsushi Takahashi,[1] Hitoshi Ikeda,[6] Hiroyuki Kuwano,[1] Seishi Ogawa[5,8] and Yasuhide Hayashi[7,8]

[1]Department of General Surgical Science, Graduate School of Medicine, Gunma University Graduate School, 3-39-15 Showa, Maebashi, Gunma 371-8511; [2]Department of Pediatrics, [3]Department of Cell Therapy and Transplantation Medicine, [4]Department of Hematology and Oncology, and [5]The 21st century COE program, Graduate School of Medicine, University of Tokyo, 7-3-1 Hongo, Bunkyo-ku, Tokyo 113-8655; [6]Department of Pediatric Surgery, Koshigaya Hospital, Dokkyo Medical School, 2-1-50 Minami-Koshigaya, Koshigaya, Saitama 343-8555; [7]Department of Hematology and Oncology, Gunma Children's Medical Center, 779 Shimohakoda, Hokkitsu, Shibukawa, Gunma 377-8577, Japan

(Received July 31, 2007/Revised November 14, 2007/Accepted November 17, 2007/Online publication January 2, 2008)

To identify the genomic profile and elucidate the pathogenesis of hepatoblastoma (HBL), the most common pediatric hepatic tumor, we performed high-density genome-wide single-nucleotide polymorphism (SNP) microarray analyses of 17 HBL samples. The copy number analyzer for GeneChip® (CNAG) and allele-specific copy number analysis using anonymous references (AsCNAR) algorithms enabled simple but sensitive inference of allelic composition without using paired normal DNA. Chromosomal aberrations were observed in 15 cases (88%). Gains in chromosomes 1q, 2 (or 2q), 8, 17q, and 20 and losses in chromosomes 4q and 11q were frequently identified. High-grade amplifications were detected at 7q34, 14q11.2, and 11q22.2. Several types of deletions, except homozygous deletion, were identified. Most importantly, copy-neutral loss of heterozygosity (uniparental disomy [UPD]) at 11p15 was detected in four of the 17 HBL samples. Insulin-like growth factor II (*IGF2*) and *H19* genes were located within this region. The methylated status of this region indicated the paternal origin of the UPD. The expression patterns of *IGF2* and *H19* were opposite between genes with and without the UPD. This difference in the expression patterns might influence the clinical features of HBL. (*Cancer Sci* 2008; 99: 564–570)

Hepatoblastoma (HBL) is the most common pediatric hepatic tumor predominantly observed in infants and children aged less than 3 years.[1–3] The dramatic increase in the survival of patients that has been observed during the last three decades is mainly due to advances in the use of chemotherapy and surgical techniques.[1–3] Currently, approximately 75% of children with HBL can be cured completely, although a large tumor, a multifocal tumor, and metastatic spread are all associated with a fatal outcome.[3] The etiology of HBL remains unknown. Most HBL are sporadic; however, an association with prematurity or low birth weight,[4] and genetic disorders such as familial adenomatous polyposis (FAP),[5] or Beckwith–Wiedemann syndrome (BWS) has been documented.[6] These findings imply that an alteration at 11p15, which is the critical region in BWS and critical to the wingless signaling pathway involving the adenomatosis polyposis coli (*APC*) gene that is constitutionally mutated in FAP patients,[7,8] could also play a role in the genesis of sporadic HBL. Indeed, the loss of heterozygosity (LOH) at 11p15 and mutations in the *APC* and β-catenin genes have also observed in some sporadic HBL.[9,10]

LOH and deletion of tumor suppressor genes are observed frequently in malignant cells and can be associated with the deregulation of cell fate and apoptosis.[11] Similarly, amplification of the chromosomal regions can increase the expression of oncogenes during tumor progression. Conventional cytogenetic analyses of chromosomal aberrations in HBL performed using standard karyotyping,[12–16] fluorescence *in situ* hybridization (FISH),[17–20] and comparative genomic hybridization (CGH),[21,22] have been reported. Although these analyses have identified several chromosomal aberrations in HBL, predominantly the gains in chromosomes 1q, 2, 8q, 17q, and 20 and the loss in chromosome 4q, the tumor-associated genes of HBL involved in these genomic copy number (CN) alterations are yet to be identified.

In recent years, a high-resolution genomic approach has been used for the systematic screening of chromosomal CN alterations. The availability of microarray-based high-density single-nucleotide polymorphism (SNP) analysis allows a reproducible and rapid determination of genome-wide alterations.[23–25] The Affymetrix® GeneChip® platform, originally developed for large-scale SNP typing, has a unique feature compared with array-based CGH: it enables the genome-wide detection of LOH in addition to extremely high-resolution CN analysis of cancer genomes by using large numbers of SNP-specific probes. The density, distribution, and allele specificity of SNP render them an excellent candidate for the high-resolution analyses of LOH and CN alterations in cancer genomes.[26,27] Conventionally, LOH analyses require the comparison of the genotypes of the tumor and its normal germline counterpart. However, for the analysis of cell line, xenograft, leukemia, and archival samples, paired normal DNA is often unavailable. In the absence of a paired normal DNA sample, LOH is inferred only based on the lower-than-expected frequencies of heterozygous SNP calls in the tumor samples. However, the low tumor content within the samples greatly hampers the sensitive detection of LOH due to increased heterozygous SNP calls. To overcome these difficulties with the current algorithms, we have recently developed novel algorithms (copy number analyzer for GeneChip® [CNAG] and allele-specific copy number analysis using anonymous references [AsCNAR]) to analyze the allelic composition of cancer genomes based on the microarray data obtained from the GeneChip® platform.[27,28] These algorithms calculate the allele-specific CN independent of the availability of a paired control DNA, enabling the sensitive detection of both LOH and CN alterations in a wide spectrum of primary tumor specimens. The performance of the new algorithm was demonstrated by detecting the neutral CN LOH or uniparental disomy (UPD) in a large number of acute leukemia samples.[28]

[8]To whom correspondence should be addressed.
E-mail: hayashiy-tky@umin.ac.jp; sogawa-tky@umin.ac.jp

doi: 10.1111/j.1349-7006.2007.00710.x

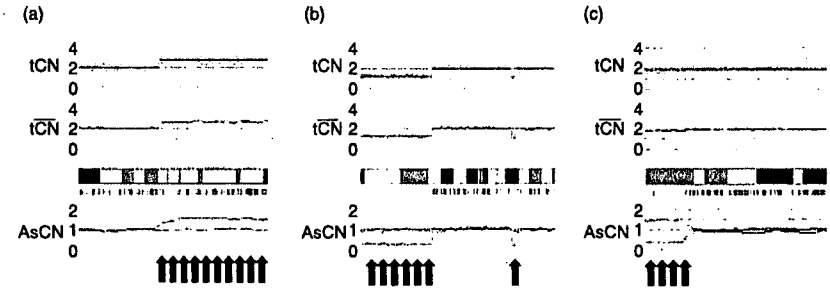

Fig. 1. Representative results of the allele-specific copy number analysis using anonymous references (AsCNAR) program with regard to copy number (CN) alterations detected in our series at particular loci, such as (a) gain (b) chromosomal loss, and (c) uniparental disomy (UPD), which have not been detected using conventional algorithms. The red dots indicate the raw CN plot for each single-nucleotide polymorphism (SNP), and the blue lines indicate the local mean CN of five SNP. The vertical green bar indicates the heterozygous SNP calls.

In the present study, to identify the novel genomic alterations in sporadic HBL cases, we performed high-resolution analyses of genome-wide CN alterations such as gains, losses, allelic imbalances, and amplifications of small chromosomal regions. Due to the high resolution of the SNP arrays and the new algorithm AsCNAR, we could systematically identify several amplifications, deletions, and allelic imbalances, including the UPD.

Materials and Methods

Patients and samples. We obtained 17 primary HBL samples at the time of diagnosis from five patients treated at the Gunma Children's Medical Center and 12 patients treated at different institutes in Japan, including Saitama Children's Medical Center. No patient had received chemo- and/or radiotherapy before the biopsy of the primary tumors. After obtaining informed consent from the parents and approval for the study from the institutional review board of each institute, all the HBL samples were subjected to genomic DNA extraction using the QIAamp DNA Mini Kit (Qiagen, Chatsworth, CA, USA) according to the manufacturer's instructions. Total RNA was extracted from the frozen stocked tumors using the Isogen reagent (Nippon Gene, Osaka, Japan), according to the manufacturer's instructions. The total RNA was reverse transcribed to synthesize cDNA using the Ready-To-Go T-Primed First-Strand Kit (GE Healthcare Bio-Sciences, Piscataway, NJ, USA).

SNP array analysis. The array experiments were performed according to the standard protocol of Affymetrix® GeneChip® Mapping 50K *Xba*I Array (Affymetrix, Inc., Santa Clara, CA, USA). In brief, the total genomic DNA (250 ng from each sample) was first digested with a restriction enzyme (*Xba*I). The digested DNA was then ligated to an appropriate adapter that recognized the four cohesive base pair (bp) overhangs, and polymerase chain reaction (PCR) amplification was performed using a single primer that recognized the adapter sequence. After fragmentation with DNase I, the PCR products were labeled with a biotinylated nucleotide analog using terminal deoxynucleotidyl transferase, and the labeled products were hybridized to the GeneChip® Human Mapping 50K Array for 17 h. Subsequently, the arrays were washed, stained, and scanned.

The genotype calls and the intensity of the SNP probes were determined using GeneChip Operation software (GCOS; Affymetrix, Inc.). The SNP CN and chromosomal regions with gains or losses were individually evaluated using the CNAG[27] and AsCNAR algorithms,[28] which enabled an accurate determination of allele-specific CN as well as the sensitive detection of LOH even in the presence of normal cell contamination of up to 70–80% without requiring constitutive DNA (Fig. 1; http://www.genome.umin.jp).

Validation of CN alterations using the interphase FISH. We performed FISH to validate the CN status obtained using the SNP array analysis. FISH probes were prepared using the BAC clones RP11-185M22, RP11-80P10, and RP11-86M15. Each BAC DNA was purified, and 100 ng of the clone was labeled with digoxigenin-dUTP using random primers; these labeled clones were used as probes for FISH analysis by following the established protocols.[29,30]

Quantitative real-time PCR and reverse transcription (RT)-PCR. Real-time quantitative PCR (RQ-PCR) and real-time quantitative RT-PCR (RQ-RT-PCR) analyses were carried out to quantify the relative CN of several amplifications in the HBL samples and the expression levels of the defender against cell death 1 (*DAD1*), EPH receptor B6 (*EphB6*), *ErbB4*, insulin-like growth factor II (*IGF2*), and *H19* genes using a Power SYBR Green PCR Master Mix (Applied Biosystems, Foster City, CA, USA) with an ABI prism 7700 real-time PCR detection system (Applied Biosystems). The primer pairs were designed using PrimerExpress software (Applied Biosystems) and synthesized by Invitrogen (Carlsbad, CA, USA).The primer sets used for the RQ-PCR experiments are listed in Table 1. Data were captured using Sequence Detection

Table 1. Primers used for polymerase chain reaction (PCR) analyses

Gene	Primer forward	Primer reverse
(Genomic RQ-PCR)		
EphB6	GGACTGCAACTGAACGTCAA	TCTGGAAAGGAAGCAAAGGA
DAD1	GTTATGTCGGCGTCGGTAGT	GTCCCCACGAGGAGACAGTA
(RQ-RT-PCR)		
ERBB4	AACAGCAGTACCGAGCCTTG	CCAGAGGCAGGTAACGAAAC
DAD1	CGAGCCTTTGCTGATTTTCT	TCCAATAAGCTGCCATCTCC
IGF2	CTCTCCGTGCTGTTCTCTCC	TATCGGGAAATGAGGTCAGC
H19	GAAGGAGGTTTAGGGGATCG	TTGCTCTTTCTGCCTGGAAC
(Bisulfite PCR/RQ-PCR)		
H19DMR (Methylated)	GGTACGGTTTTTTTAGGTTTATGTC	ACCCCTACAACCTCCTTACTACG
H19DMR (Unmethylated)	TATGGTTTTTTTAGGTTTATGTTGG	ACCCCTACAACCTCCTTACTACAC

Primers and probes were designed using Primer Express software and MethPrimer software. RQ-PCR, real-time quantitative PCR; RQ-RT-PCR, real-time quantitative reverse transcription-PCR.

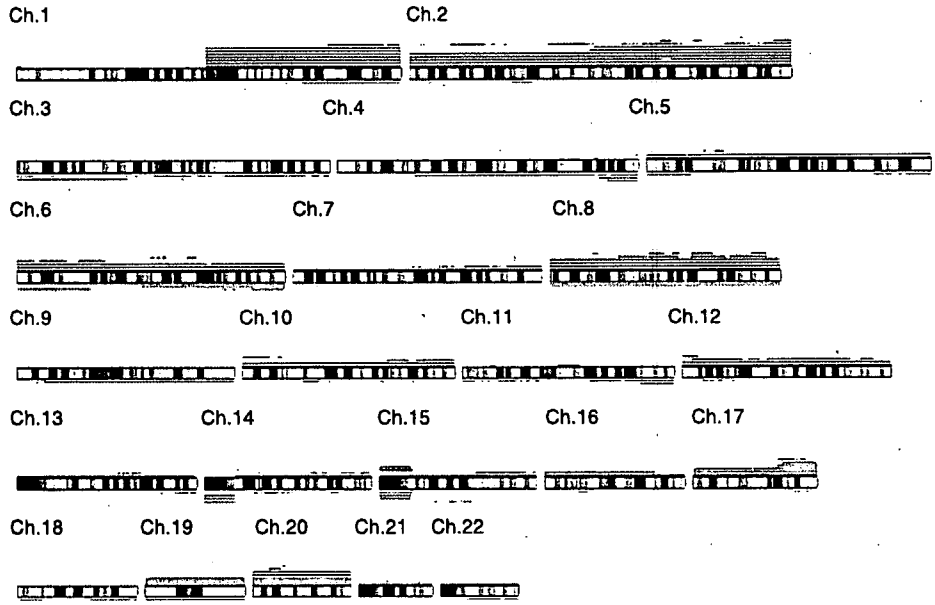

Fig. 2. Overview of the DNA copy number (CN) gains and losses detected in 17 hepatoblastoma (HBL) samples. A gain is indicated by the red bar above the chromosome ideogram, and a loss is indicated by the green bar under the chromosome ideogram. Each horizontal line represents an aberration detected in a single tumor.

software (version 1.7a; Applied Biosystems). For each primer pair, a standard curve was generated from five-fold serial dilution from approximately 50–80 pg of control DNA from a healthy individual. The amounts of genomic DNA and cDNA used in each test and the reference marker for all HBL samples were calculated using the appropriate standard curve. Normalization was performed using the β-actin gene as the internal control.

Sodium bisulfite modification and methylation-specific PCR. The genomic DNA from the tumor samples was treated with sodium bisulfite as described previously.[31] Briefly, 1 μg of DNA was denatured with sodium hydroxide and modified with sodium bisulfite. The modified DNA was then purified with the Wizard® DNA Clean-Up System (Promega, Madison, WI, USA), precipitated with ethanol, resuspended in Tris-EDTA (TE) buffer (pH 8.0), and either used immediately or stored at −20°C until use. The bisulfite-modified DNA was amplified with primer pairs for the methylated and unmethylated complete sequences upstream of the *H19* promoter CpG islands in the HBL samples with UPD in 11p15. The primer pairs were designed using MethPrimer software,[32] and synthesized by Invitrogen. The primers for methylation-specific DNA and unmethylation-specific primers are listed in Table 1. Normal lymphocyte DNA was used as the control. PCR was carried out in a 25 μL reaction volume using Ex Taq Hot Start Version (TaKaRa Bio Inc., Kyoto, Japan). The PCR conditions were as follows: 1 cycle at 95°C for 10 min; followed by 35 cycles of 94°C for 30 s, 60°C for 30 s, 72°C for 2 min; and a final extension at 72°C for 5 min. The PCR products were separated on 3% agarose gels and visualized under UV illumination after ethidium bromide staining. To quantify the ratio of the methylation status, we also carried out the methylation-specific RQ-PCR analysis.

Results

Detection of CN alterations in HBL samples. We investigated 17 HBL samples obtained from the sporadic cases of HBL by using the Affymetrix® GeneChip® 50K *Xba*I Mapping Array. Although these specimens did not contain paired control DNA and had varying degrees of normal tissue contamination, the genomic alterations were accurately determined in most specimens by our CNAG/AsCNAR program (Fig. 1). The real CN and LOH status was inferred from the observed signal ratios of the tumor to the reference, based on the hidden Markov models implemented in the CNAG/AsCNAR program; these are summarized in Fig. 2. The CN data were validated at a number of SNP sites using FISH analysis of the cell nuclei extracted from the HBL samples (Fig. 3). The CN data obtained using the FISH analyses were consistent with those obtained using SNP mapping.

Numerical chromosomal aberrations were observed in 15 HBL samples (88%), excluding two HBL samples (HBL_22 and HBL_250). These 15 cases had variable degrees of CN gains and losses; however, the gains including the amplifications were more frequent than the losses (Table 2 and Fig. 2). Total or partial gains in chromosomes 1q and 2 were the most frequent aberrations detected in eight of the 17 patients (47%). The gain in chromosome 8 was the second most frequent aberration detected in five of the 17 samples (29%). The gains in chromosomes 17q and 20 were observed in 24% of the cases (four of 17 cases). The LOH in chromosomes 4q and 11q was observed in three (18%) and two (12%) of the 17 samples, respectively. However, these regions were usually large, and we could not determine the presence or absence of alterations in specific genes within these regions.

High-grade amplification and common deletion. High-grade amplifications are of particular interest because they may indicate the loci of oncogenes. The regions with high-grade amplification were defined as segments with at least five SNP loci with an inferred CN of >5. High-grade amplifications of 7q34 and 14q11.2 were observed in five (29%) and nine (53%) HBL samples, respectively. For the validation of the amplifications observed using the SNP array, FISH analysis and genomic RQ-PCR were performed. To determine the genes that are potentially affected at 14q11.2, several genes localized at the 14q11.2 chromosomal region with overlap or proximity to the BAC-RP11-85M16 were examined using the UCSC browser (www.genome.ucsc.edu). Genes that map to these regions include *EphB6* and *DAD1*, which are identified as the negative regulators of apoptosis. These two genes were subjected to RQ-PCR. FISH analysis with RP11-85M16 BAC clone probe showed multiple signals, confirming

doi: 10.1111/j.1349-7006.2007.00710.x

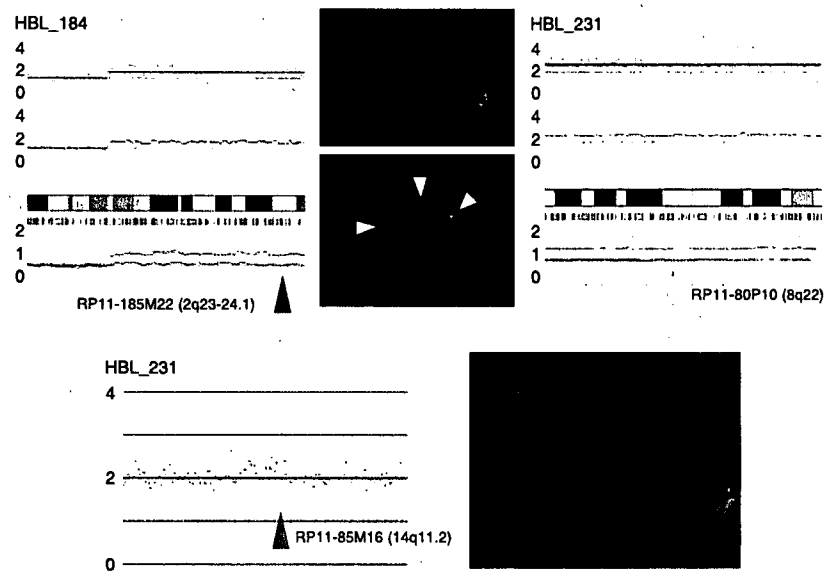

Fig. 3. Representative results of array analysis of hepatoblastoma (HBL) samples (HBL_184 and HBL_231). Fluorescent *in situ* hybridization analysis with BAC probes confirmed the detected changes. We detected three signals from chromosomes 2q and 8q. At the high-amplification region of chromosome 14q, three and more signals were detected.

Table 2. Chromosomal aberrations in 17 primary hepatoblastoma (HBL) samples

Sample	Copy number gain	Copy number loss	Uniparental disomy
HBL_4	1q, 2q34, 5p13.1, 17q23.3-qter	3p13-pter, 3q13.11, 6q14.1-qter, 11q23.1-qter	Not detected
HBL_7	1q, 2, 8, 14q11.2, 20	not detected	11p15.4-pter
HBL_8	7q34	not detected	Not detected
HBL_9	1q, 2q14.1-qter, 6p, 7, 14q11.2	6p12.1, 9p21.1	Not detected
HBL_12	8q11.23, 10q21.3, 10q26.13, 14q11.2, 22q13.31	7q35	Not detected
HBL_14	2p16.3-p22.3, 2p23.1, 2q11.2-q14.1, 2q33.1-q34, 3p21.33-p22.1, 3p24.2, 3p25.1, 3p25.2, 4q32.2-q32.3, 5p13.2, 6q14.3-q16.1, 7q, 11p15.1, 10p13-pter, 11q22.2-q22.3, 12p13.2-pter, 14q23.3-q31.1, 15q22.31-q26.2, 16p12.3, 20p11.23	1q31.1-qter, 2p12-14, 3, 4q, 5p14.1-pter, 5q32-qter, 6p12.13-pter, 6q11.1, 6q25.1-qter, 8, 9, 12p11.1-13.1, 17q24.3, 18p11.21-11.32, 18q21.1-qter, 19, 22	Not detected
HBL_22	Not detected	Not detected	Not detected
HBL_27	1q, 2q24.2-24.3, 7q34, 14q11.2	4q32.3-qter, 16p12.1	Not detected
HBL_28	3p26.1, 7q34, 14q11.2, 20	2p24.1	11p14.3-pter
HBL_34	1q, 2, 7q34, 14q11.2, 17	4q34.1-qter	Not detected
HBL_36	1q32.1-qter	1p13.3-pter, 4q21.22-qter, 5p13.1	Not detected
HBL_37	1q, 2, 5, 6, 7q34, 8, 10, 12, 14, 14q11.2, 15, 16q22.1-pter, 17, 19, 20	Not detected	11p15.2-pter, 16q22.2-qter
HBL_184	2q14.2-qter, 3p24.3, 4q33, 10p14, 11p14.3, 14q11.2	Not detected	Not detected
HBL_185	6p, 21q21.2	Not detected	Not detected
HBL_231	8, 14q11.2, 19, 20	Not detected	11p15.4-pter
HBL_246	1q, 2, 5, 6, 8, 10, 12, 13, 16, 17, 19, 20, 21, 22	Not detected	4, 9
HBL_250	Not detected	Not detected	Not detected

CN gains at 14q11.2 (Fig. 3). Further, in RQ-PCR analysis, the CN gain of *EphB6* and *DAD1* was evident in all samples that showed high-grade amplification in SNP array (data not shown). Other high-grade amplifications are listed in Table 3. The size of these amplicons was typically less than 1 Mb, and the possible genes present in these regions are summarized in the same table. All these candidate genes, except *MMP7*, have not been reported previously with regard to HBL.[33]

Homozygous deletions are also of particular interest because they may indicate a tumor suppressor gene. However, homozygous deletions were not identified in any sample.

CN neutral LOH (UPD). LOH can be more sensitively detected with the CNAG/AsCNAR algorithms by evaluating the allele-specific CN than from the grossly reduced heterozygous SNP calls, particularly when the SNP shows no CN losses. The UPD regions were identified in five of the 17 samples. In four samples (HBL_7, HBL_28, HBL_37, and HBL_231), 11p15 was the common UPD region (Fig. 4a). Other UPD regions were observed within chromosomes 4, 9, and 16q22 (Table 2). The candidate target genes that map to the UPD region located within 11p15 include *IGF2* and *H19*. Methylation-specific PCR analysis was performed for the four HBL samples having UPD within 11p15 to identify the origin of the amplified allele. The methylation status of the differential methylated region (DMR) of *H19* is shown in Fig. 4b. Hypermethylation of the *H19* DMR was detected in all HBL samples having UPD within 11p15; however, normal lymphocyte DNA showed the mosaic methylation pattern. In general, the *H19* DMR is hypermethylated on the paternal allele

Table 3. High-grade amplifications in hepatoblastoma (HBL) samples

Cytoband	Implicated region (base pairs)		Candidate target genes in the region
	Start–end	Size	
2q34	211 193 864–212 239 181	1 045 318	*ErbB4*
3p25.2	11 888 124–12 876 175	988 052	*RAF1*
7q34	141 721 559–142 076 238	354 680	*EphB6*
11q22.2-q22.3	101 394 973–102 830 195	1 435 223	*MMP1, 7, 20*
14q11.2	21 426 631–22 130 392	703 762	*DAD1*

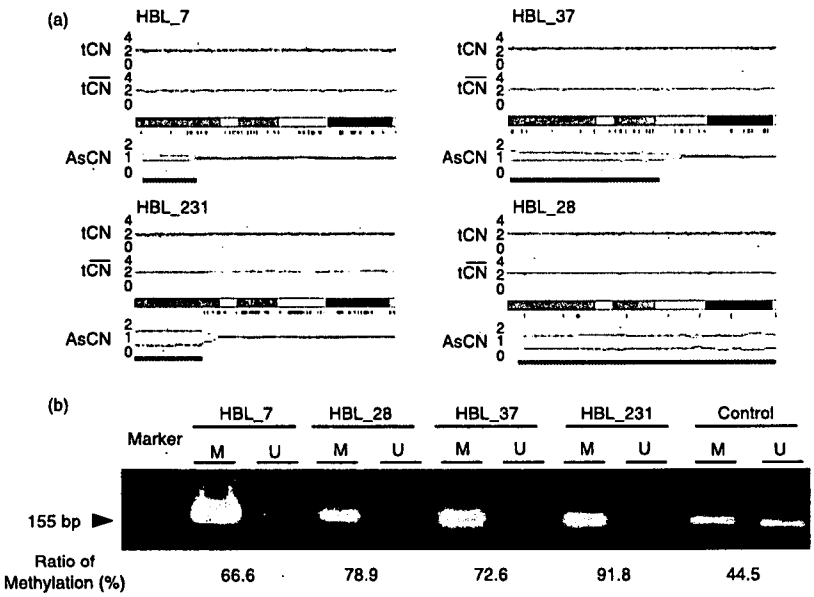

Fig. 4. (a) Copy numbers (CN) of chromosome 11p in four hepatoblastoma (HBL) samples with uniparental disomy (UPD). Although complete CN alterations are not observed, UPD is clearly predicted based on the allele-specific CN alterations (green lines). (b) Methylation-specific polymerase chain reaction (PCR) analysis of the *H19* differential methylated region (DMR). Modified DNA was amplified with primer pairs for methylated and unmethylated complete sequences of the *H19* DMR. *H19* DMR hypermethylation was detected in all HBL samples; however, normal lymphocyte DNA exhibited the mosaic methylation pattern. The results of quantitative real-time methylation-specific PCR analysis are shown below the image depicting the results of electrophoresis.

and hypomethylated on the maternally expressed allele in humans. This indicates that the UPD within this region is considered to be derived from the paternal allele. Furthermore, a low expression level of the non-methylated allele was also observed; methylation-specific RQ-PCR analysis revealed that the ratio of the methylation status ranged from 66.6% to 91.8%.

Expression analyses using RQ-RT-PCR. In order to examine the impact of the abovementioned amplifications and UPD on gene expression, we measured the expression levels of four genes (*DAD1*, *ErbB4*, *IGF2*, and *H19*) through RQ-RT-PCR (Fig. 5). Normal liver total RNA served as the non-neoplastic reference and control. HBL_184 and HBL_231 for which RNA were available showed a high expression of the *ErbB4* gene. However, the expression of *DAD1* was down-regulated in both these samples. The *IGF2* and *H19* genes were oppositely expressed between HBL_184 and HBL_231, having UPD within 11p15.

Discussion

The present study represents the application of the SNP array technology for the genome-wide analysis of CN aberrations in HBL. Several recent studies and our previous research have demonstrated that this technology provided a unique opportunity to assess the DNA CN alterations and LOH simultaneously throughout the entire genome.[24–27,29] As shown in the present analysis, the use of high-resolution SNP arrays improved the ability to identify structural chromosomal aberrations in cancer cells and detect genes affected by these aberrations. Additionally, high-density SNP array analysis with the CN analyzer software can also

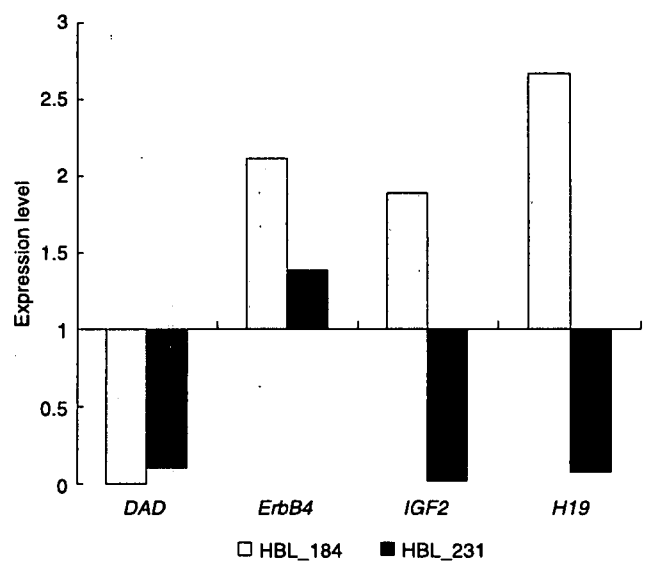

Fig. 5. The results of the expression levels of four genes (defender against cell death 1 [*DAD1*], EPH receptor B6 [*EphB6*], *ErbB4*, insulin-like growth factor II [*IGF2*], and *H19* genes) through real-time quantitative reverse transcription-polymerase chain reaction (RQ-RT-PCR) analyses.

doi: 10.1111/j.1349-7006.2007.00710.x